A&A 482, 945–960 (2008)
DOI: 10.1051/0004-6361:20066176
© ESO 2008

Astronomy & Astrophysics

Mass loss from late-type WN stars and its *Z*-dependence

Very massive stars approaching the Eddington limit

G. Gräfener and W.-R. Hamann

Institut für Physik, Universität Potsdam, Am Neuen Palais 10, 14469 Potsdam, Germany
e-mail: goetz@astro.physik.uni-potsdam.de

Received 3 August 2006 / Accepted 1 February 2008

ABSTRACT

Context. The mass loss from Wolf-Rayet (WR) stars is of fundamental importance for the final fate of massive stars and their chemical yields. Its Z-dependence is discussed in relation to the formation of long-duration Gamma Ray Bursts (GRBs) and the yields from early stellar generations. However, the mechanism of formation of WR-type stellar winds is still under debate.
Aims. We present the first fully self-consistent atmosphere/wind models for late-type WN stars. We investigate the mechanisms leading to their strong mass loss, and examine the dependence on stellar parameters, in particular on the metallicity Z.
Methods. We perform a systematic parameter study of the mass loss from WNL stars, utilizing a new generation of hydrodynamic non-LTE model atmospheres. The models include a self-consistent treatment of the wind hydrodynamics, and take Fe-group line-blanketing and clumping into account. They thus allow a realistic modelling of the expanding atmospheres of WR stars. The results are verified by comparison with observed WNL spectra.
Results. We identify WNL stars as very massive stars close to the Eddington limit, potentially still in the phase of central H-burning. Due to their high L/M ratios, these stars develop optically thick, radiatively driven winds. These winds show qualitatively different properties than the thin winds of OB stars. The resultant mass loss depends strongly on Z, but also on the Eddington factor Γ_e, and the stellar temperature $T_\star$. We combine our results in a parametrized mass loss recipe for WNL stars.
Conclusions. According to our present model computations, stars close to the Eddington limit tend to form strong WR-type winds, even at very low Z. Our models thus predict an efficient mass loss mechanism for low metallicity stars. For extremely metal-poor stars, we find that the self-enrichment with primary nitrogen can drive WR-type mass loss. These first WN stars might play an important role in the enrichment of the early ISM with freshly produced nitrogen.

Key words. stars: Wolf-Rayet – stars: early-type – stars: atmospheres – stars: mass-loss – stars: winds, outflows – stars: individual: WR 22

1. Introduction

The strong mass loss from Wolf-Rayet (WR) stars fundamentally affects the evolution, the final fate, and the chemical yields of the most massive stars. Its dependence on metallicity (Z) received renewed interest because of the possible importance for early generations of massive stars and their chemical yields (see Meynet et al. 2006; Chiappini et al. 2006). Moreover, within the collapsar model (Woosley et al. 1993; MacFadyen & Woosley 1999), fast rotating WR stars are now broadly accepted as the progenitors of long-duration Gamma Ray Bursts (GRBs). The formation of GRB progenitors with the demanded properties could be explained by lowered WR mass loss rates at low metallicities (Yoon & Langer 2005; Woosley & Heger 2006).

Despite their importance, the mechanism of formation of WR-type stellar winds is still under debate. The high WR luminosities and surface temperatures suggest that WR winds are driven by radiation. The observed wind performance numbers $\eta = \dot{M}v_\infty/(L_\star/c)$, on the other hand, appear to challenge this hypothesis. Commonly observed values in the range $\eta = 1-10$ imply a mechanical wind momentum much in excess of the momentum of the radiation field. If WR winds are driven by radiation, photons must be used more than once. This can either be achieved by multiple line scattering, or by successive redistribution and absorption of thermalized photons.

The question of the driving mechanism of WR mass loss is strongly related to its dependence on metallicity (Z). If WR winds are driven by radiation, one would expect a similar Z-dependence as for the radiatively driven winds of OB stars. Such a relation has recently been claimed by Vink & de Koter (2005) for the winds of late WR subtypes (WNL and WCL). Because of the absence of observations over a broad metallicity range, computational wind models are needed to address these questions. However, as previously mentioned, WR winds are far from being fully understood. Consequently only a few models are available, partly based on controversial model assumptions.

The first models for WR winds were constructed by Lucy & Abbott (1993) and Springmann (1994), using Monte-Carlo techniques. These authors could show that multiple line scattering can account for the high observed wind performance numbers (up to $\eta \approx 10$) if enough line opacities are present. However, the models could not prove whether WR winds are entirely driven by radiation, because they rely on an adopted velocity structure, without solving the wind hydrodynamics. In particular the models failed to reproduce the wind acceleration in deep atmospheric layers. The WNL models by de Koter et al. (1997) and

the Z-dependent models by Vink & de Koter (2005) are based on a similar modelling technique where the ionization conditions in the extended WR atmospheres are inferred from model atmosphere grids. Also these models cannot explain the wind driving in deep layers.

A completely different approach was followed by Nugis & Lamers (2002) and Lamers & Nugis (2002). By means of a critical-point analysis these authors could show that the observed WR mass loss rates are in agreement with the assumption of optically thick, radiatively driven winds. In this approach it is assumed that the sonic point is located in very deep atmospheric layers where the diffusion limit is valid (note that under this assumption the sonic point becomes the critical point of the wind flow). Nugis & Lamers found that the sonic point must be located in specific temperature regimes where the Rosseland mean opacity is increasing due to the well-known Fe opacity peaks (cf. Iglesias & Rogers 1996). In this picture, late-type WR winds are initiated by the "cool Fe-peak" (for sonic point temperatures of T_s = 40−70 kK), whereas the winds of early subtypes are supported by the "hot Fe-peak" (T_s > 160 kK).

Our own approach follows a computationally much more expensive path, where the full wind is modeled in a self-consistent manner. For this purpose a hydrodynamic solution scheme is incorporated into the Potsdam Wolf-Rayet (PoWR) atmosphere models. Within these models a detailed non-LTE radiative transfer is performed, which takes Fe-group line-blanketing and wind clumping into account. They are thus able to describe the conditions in the WR wind, including the optically thick part, in a realistic manner (see Sect. 3 for a detailed description of the PoWR models). Using these models we could show that it is in principle possible to drive a strong WR wind by radiation pressure alone (Gräfener & Hamann 2005). In accordance with Nugis & Lamers (2002), we found that the inner wind regions of early-type WC stars are supported by line opacities from the hot Fe-peak (ionization stages Fe IX−Fe XVI), and that the observed mass loss rates can only be reached for extremely high critical-point temperatures (≈200 kK). Moreover, we could demonstrate the importance of clumping in the wind dynamics, an effect which has not been taken into account in any previous wind calculation.

In the present work we focus on late-type WN stars (WNL stars, spectral subtypes WN 6-9). Compared to early subtypes, these stars have rather low effective temperatures (30−60 kK) in a similar range as, e.g., typical O supergiants. Hamann et al. (2006) recently found that these stars form a distinct group within the galactic WN population, with exceptionally high luminosities (above $\sim 10^{5.9}\ L_\odot$). This result is in line with previous detections of very high luminosities for H-rich WNL subtypes in the LMC (de Koter et al. 1997; Crowther & Dessart 1998), and the galactic center (Najarro et al. 2004). Here we investigate the question of why these stars show enhanced, WR-type mass loss, and present a grid of WNL wind models for different metallicities. Moreover, we examine the possibility of strong WR-type mass loss for the earliest generations of metal-poor massive stars, as a result of self-enrichment with primary nitrogen (see Meynet et al. 2006).

In Sect. 2 we give a short overview of the applied modelling technique and the adopted atomic data. In Sect. 3 we present the results of our model computations and compare them with observations. In Sect. 4 we discuss the specific properties of WR-type winds, and relate them to previous mass loss studies. Finally, we discuss the most important implications of our results in Sect. 5, and summarize the main conclusions in Sect. 6.

2. Atmosphere models

The Potsdam Wolf-Rayet (PoWR) model atmosphere code is a state-of-the-art code for expanding stellar atmospheres, which incorporates the treatment of line-blanketing due to millions of Fe-group transitions in non-LTE (for details of the numeric treatment see Koesterke et al. 1992; Hamann et al. 1992; Leuenhagen & Hamann 1994; Koesterke & Hamann 1995; Leuenhagen et al. 1996; Hamann & Koesterke 1998a; Koesterke et al. 2002; Gräfener et al. 2002; Hamann & Gräfener 2003). Within our group this code has been extensively applied to the quantitative analysis of WR stars (Gräfener et al. 2000, 2002; Gräfener et al. 2002; Hamann et al. 2003; Stasińska et al. 2004; Hamann et al. 2006; Barniske et al. 2006). Recently the code was extended by a self-consistent solution of the hydrodynamic equations (Gräfener & Hamann 2005), where the atmosphere structure ($\rho(r)$ and $v(r)$) is determined consistently with the radiative acceleration as obtained from the non-LTE radiation transport.

Here we give an overview of the applied modelling technique. In Sect. 2.1 we describe the applied numerical methods, in Sect. 2.2 we review the relevant model parameters, and in Sect. 2.3 we summarize the atomic data utilized for the calculations.

2.1. Numerical methods

The model code computes the radiation field, the atomic level populations, the temperature structure, the density structure, and the velocity field for a stationary, spherically expanding stellar atmosphere. The complete solution comprises four parts which are iterated until consistency is obtained: the radiation transport, the equations of statistical equilibrium, the energy equation, and the hydrodynamic equations.

The radiation transport for a spherically expanding atmosphere is formulated in the co-moving frame of reference (CMF), neglecting aberration and advection terms (see Mihalas et al. 1976). For a fast solution and a consistent treatment of electron scattering we employ the method of variable Eddington factors (Auer & Mihalas 1970). This means that the moment equations are solved to obtain the angle-averaged radiation field, and the numerically expensive ray-by-ray transfer is only calculated from time to time (Koesterke et al. 2002; Gräfener et al. 2002). The fast numerical solution allows a detailed treatment of millions of spectral lines on a fine frequency grid.

The atomic populations and the electron density are determined from the equations of statistical equilibrium. This system of equations is solved in line with the radiation transport by application of the ALI formalism (accelerated lambda iteration, see Hamann 1985, 1986). Complex model atoms of He, C, N, O, Si, and the Fe-group are taken into account. For the inclusion of millions of iron-group transitions we take advantage of the super-level concept following Anderson (1989). The details of the numerical implementation are described by Gräfener et al. (2002). Density inhomogeneities are taken into account in the limit of small-scale clumps, or micro-clumping (see Hamann & Koesterke 1998a, and Sects. 4.2 and 5.3 in the present work). The clumping factor D denotes the density enhancement within a clump, or the inverse of the volume filling factor f_V.

The temperature structure is obtained from the assumption of radiative equilibrium. In the present work this constraint equation is decoupled from the equations of statistical equilibrium. It is solved by a temperature correction procedure which is based on the Unsöld-Lucy method (Unsöld 1955; Lucy 1964), and has

been generalized for application in non-LTE models with spherical expansion (Hamann & Gräfener 2003).

The density- and velocity structure of the expanding atmosphere is obtained from the hydrodynamic equations for a stationary radial flow, accelerated by radiation pressure (see Gräfener & Hamann 2005). The radiative acceleration is obtained by direct integration within the CMF radiation transport

$$a_{\rm rad} = \frac{1}{\rho}\frac{4\pi}{c}\int_0^\infty \kappa_\nu H_\nu \, {\rm d}\nu, \qquad (1)$$

where the Eddington flux H_ν and the opacity κ_ν are both computed on a fine frequency grid.

Due to Doppler shifts, the radiative acceleration on spectral lines reacts to changes of the velocity gradient v'. Because of its influence on the dynamic properties of the gas flow, this dependence must be included in the hydrodynamic solution. In our computations we perform an additional radiative transfer calculation in advance of each hydro-iteration, where the velocity distribution $v(r)$ is changed. In this way we determine the fraction of $a_{\rm rad}$ that responds linearly to small variations of v'. This value corresponds to the effective contribution of optically thick spectral lines ($a_{\rm thick}$) to the total radiative acceleration (see, e.g., Puls et al. 2000). Dividing $a_{\rm thick}$ by the total acceleration from spectral lines ($a_{\rm lines}$) gives the force multiplier parameter α, which has a similar meaning as the parameter α in the standard theory of line driven winds by Castor et al. (1975, CAK). Note, however, that our α is an *effective* value which includes complex effects like line overlaps and changes in the wind ionization, while the CAK α is deduced from atomic line statistics.

2.2. Model parameters

Our hydrodynamic model atmospheres are characterized by the mass, the luminosity, the radius, and the chemical composition of the stellar core. Moreover, the clumping factor must be prescribed throughout the wind. Given these parameters, the density and velocity structure of the atmosphere follow from the hydrodynamic solution. The basic model parameters are: the stellar core radius $R_\star$ at Rosseland optical depth $\tau_{\rm R} = 20$, the stellar temperature $T_\star$ (related to the luminosity $L_\star$ and the core radius $R_\star$ via the Stefan Boltzmann law), the stellar mass $M_\star$, the chemical composition, and the clumping factor D which is prescribed as a function of $\tau_{\rm R}$. Note that we define $\tau_{\rm R}$ in this context as the "LTE-continuum" Rosseland mean optical depth.

For the line broadening we assume Doppler profiles with a broadening velocity of $v_{\rm D} = 100\ {\rm km\,s^{-1}}$ throughout this work. In this way the absorption troughs of P-Cygni type line profiles are successfully reproduced. Moreover, we are presently limited to relatively high broadening velocities because the frequency spacing in our models scales with $v_{\rm D}$, and the computation time thus scales with $1/v_{\rm D}$.

Because of its effect on the radiative acceleration, the detailed prescription of the clumping factor $D(r)$ has an influence on the obtained results. Unfortunately, this value can only be constrained very roughly from the observed electron scattering wings of strong emission lines (see Hamann & Koesterke 1998a). For the outer part of the wind we thus adopt a constant value of $D_{\rm max} = 10$, which gave satisfactory results in previous analyses of similar stars (e.g., Herald et al. 2001; Martins et al. 2008). For the radial dependence in the deeper wind layers we rely on previous results for WR 111 (Gräfener & Hamann 2005) where a τ-dependent formulation reproduces high ionization stages very well, which are formed deep inside the atmosphere. In this formulation D continuously increases from a value of $D_{\rm min} = 1$ at the wind base (for $\tau_{\rm R} > 0.7$) to $D_{\rm max} = 10$ in the outer layers (for $\tau_{\rm R} < 0.35$).

The freedom in the prescription of $D(r)$ is not satisfactory. However, clumping is clearly detected in WR winds and should be included in the models. As long as only optically thin regions above the critical point of the equation of motion are affected by clumping, its influence on the obtained mass loss rates is relatively small (see Sect. 4.2). Nevertheless, we expect a strong influence on the outer wind structure and in particular on the terminal wind velocities.

Table 1. Summary of the model atom. Fe-group ions (Fe) are described by a relatively small number of super-levels, each representing a large number of true atomic energy levels (sub-levels). The relative abundances of the Fe-group elements are listed in Gräfener et al. (2002), Table 2.

Ion	Levels	Ion	Levels	Ion	Super-levels	Sub-levels
H I	10	N IV	44	Fe I	1	21
H II	1	N V	17	Fe II	12	17 170
He I	17	N VI	1	Fe III	16	14 188
He II	16	O II	3	Fe IV	18	30 122
He III	1	O III	9	Fe V	19	19 804
C I	1	O IV	8	Fe VI	18	15 155
C II	3	O V	12	Fe VII	16	11 867
C III	12	O VI	9	Fe VIII	17	8669
C IV	9	O VII	1	Fe IX	19	12 366
C V	1	Si III	10	Fe X	1	1
N I	3	Si IV	7			
N II	38	Si V	1			
N III	40					

2.3. Atomic data

The chemical composition of the model atmospheres is given by the mass fractions $X_{\rm He}$, $X_{\rm C}$, $X_{\rm N}$, $X_{\rm O}$, $X_{\rm Si}$, and $X_{\rm Fe}$ of helium, carbon, nitrogen, oxygen, silicon, and iron-group elements. Compared to our previous models for early-type WC stars (Gräfener et al. 2002; Stasińska et al. 2004; Gräfener & Hamann 2005) we have reduced the model atoms significantly. This is possible because of the lower effective temperatures, and the specific chemical composition of WN stars (mainly H, He, and N). In particular, we use rather small atomic models for carbon and oxygen, and a reduced number of ionization stages for the iron group (Fe I–X). In this way we manage to combine the most relevant atomic species in a model atom with 410 super levels. This model atom still allows moderate computing times of the order of 1–3 days for a hydrodynamic model, i.e., it permits parameter studies with a large number of grid models.

The model atoms are summarized in Table 1. The atomic data are compiled from the following sources. Oscillator strengths for CNO are taken from the Opacity Project (Hummer & Mihalas 1988; Seaton 1987; Seaton et al. 1992; Cunto & Mendoza 1992; Seaton et al. 1994; The Opacity Project Team 1995), level energies from Kurucz's CD-ROM No. 23 (Kurucz & Bell 1995), and ionization cross sections from Nahar & Pradhan (1997) and Nahar (1999). Fe-group data are taken from Kurucz CD-ROM Nos. 20–22 (see Kurucz 1991, 2002).

3. Model calculations

In this section we present a systematic parameter study of the mass loss from late-type WN stars. The first question

Table 2. Model parameters for our different (grid) computations. The first column (Grid 1) denotes the models from Sect. 3.1 for solar Z, where $T_\star$ and Γ_e are varied. In the second column the parameters for the WR 22 model from Sect. 3.2 are given. The third column (Grid 2) indicates our Z-dependent models from Sect. 3.3, followed by the computations for extremely metal-poor stars with zero Fe abundance (Grid 3). The next two columns belong to Sect. 3.4 where the dependence on X_H (Grid 4) and $L_\star$ (Grid 5) are investigated. The last column (VdK05) indicates a model from Sect. 4.3 for comparison with the WNL model from Vink & de Koter (2005) for solar Z. Note that for the Z-dependent models $z = Z/Z_\odot$ indicates the relative mass fraction of metals with respect to the solar value. The luminosity $L_\star$, the radius $R_\star$, the temperature $T_\star$, and the mass $M_\star$ of the stellar core (with the corresponding Eddington factor Γ_e), the assumed maximum wind clumping factor D_{max}, the surface mass fractions X_{He}, X_C, X_H, X_O, X_{Si}, and X_{Fe}, and the resultant mass loss rates $\dot{M}$, transformed radii R_t, terminal wind velocities v_∞, and wind efficiencies $\eta = \dot{M}v_\infty/(L_\star/c)$ are given.

Models	Grid 1: $T_\star$, Γ_e	WR 22	Grid 2: Z, Γ_e	Grid 3: $X_{Fe} = 0$	Grid 4: X_H, $T_\star$	Grid 5: $L_\star$, $T_\star$	VdK05
$L_\star/L_\odot$	$10^{6.3}$	$10^{6.3}$	$10^{6.3}$	$10^{6.3}$	$10^{6.3}$	$10^{5.1...6.6}$	$10^{5.6}$
$R_\star/R_\odot$	47.2 ... 11.9	23.7	23.7	23.7	18.8 ... 47.2	4.7 ... 66.7	13.5
$T_\star$/kK	31.6 ... 63.1	44.7	44.7	44.7	31.6 ... 50.1	31.6 ... 50.1	40.0
$M_\star/M_\odot$	67, 55	78.1	101 ... 48.4	59.3 ... 49.1	55.8 ... 100.4	4.9 ... 155.9	20.0
Γ_e	0.55, 0.67	0.55	0.44 ... 0.89	0.73 ... 0.88	0.55	0.55	0.37
D_{max}	10	10	10	10	10	10	10
X_H	0.2	0.4	0.4	0.4	0.0 ... 0.8	0.4	0.15
X_{He}	0.78	0.58	0.58	0.58	0.18 ... 0.98	0.58	0.83
X_C	4.0×10^{-4}	4.0×10^{-4}	$4.0 \times 10^{-4} \cdot z$	4.0×10^{-4}	4.0×10^{-4}	4.0×10^{-4}	4.0×10^{-4}
X_N	1.4×10^{-2}	1.4×10^{-2}	$1.4 \times 10^{-2} \cdot z$	1.4×10^{-2}	1.4×10^{-2}	1.4×10^{-2}	1.4×10^{-2}
X_O	1.0×10^{-3}	1.0×10^{-3}	$1.0 \times 10^{-3} \cdot z$	1.0×10^{-3}	1.0×10^{-3}	1.0×10^{-3}	1.0×10^{-3}
X_{Si}	8.0×10^{-4}	8.0×10^{-4}	$8.0 \times 10^{-4} \cdot z$	0	8.0×10^{-4}	8.0×10^{-4}	8.0×10^{-4}
X_{Fe}	1.6×10^{-3}	1.6×10^{-3}	$1.6 \times 10^{-3} \cdot z$	0	1.6×10^{-3}	1.6×10^{-3}	1.6×10^{-3}
$\dot{M}/\ M_\odot\ \mathrm{yr}^{-1}$	$10^{-(4.1 ... 5.0)}$	$10^{-4.85}$	$10^{-(4.6 ... 5.4)}$	$10^{-(4.7 ... 5.5)}$	$10^{-(4.2 ... 5.2)}$	$10^{-(4.2 ... 5.5)}$	$10^{-(5.41)}$
$v_\infty/\ \mathrm{km\,s}^{-1}$	778 ... 1298	974	240 ... 1903	388 ... 478	646 ... 1396	620 ... 1567	941
$R_t/R_\odot$	9.6 ... 20.6	21.7	9.2 ... 53.7	9.1 ... 37.7	12.5 ... 39.7	8.02 ... 30.7	28.2
η	0.28 ... 1.51	0.34	0.04 ... 1.15	0.04 ... 0.21	0.20 ... 1.12	0.20 ... 1.72	0.44

concerning these objects is *why* they become WR stars, i.e., why they show enhanced mass loss. We address this question in Sect. 3.1, where we investigate the dependence of WNL mass loss on stellar parameters, and compare our results with observed properties of the galactic WNL sample. In Sect. 3.2 we perform a more detailed comparison with WR 22, a spectroscopic binary for which the mass of the WR component is roughly known. Finally, we investigate the Z-dependence of WNL star mass loss in Sect. 3.3, and combine our results in the form of a mass loss recipe in Sect. 3.4.

3.1. WNL stars at solar metallicity

A large part of the galactic WN population has been re-analyzed by Hamann et al. (2006), based on a publicly accessible grid of line-blanketed atmosphere models (Hamann & Gräfener 2004, http://www.astro.physik.uni-potsdam.de). In this study the WN parameters have been significantly revised (e.g., compared to Hamann & Koesterke 1998b), chiefly due to the influence of Fe-group line-blanketing, and the consideration of 2MASS IR photometry. In particular, the galactic WN stars are now found to form two distinct groups which are divided by their luminosities. The first group consists of a mixture of early- to intermediate WN subtypes with luminosities below $10^{5.9}\ L_\odot$. The second group, formed by the WNL stars (WN 6–9), shows luminosities above this value. While the earlier subtypes are dominated by pure He-stars, WNL stars tend to show a significant amount of hydrogen at their surface (up to $X_H = 0.55$). They are located to the right of the zero-age main-sequence in a temperature range of $T_\star = 35{-}55$ kK, and thus might still be in the phase of central H-burning. In the present work we concentrate on this class of extremely luminous evolved stars, which are in many cases among the most luminous objects in young stellar clusters.

Our main goal now is to show why these stars become WR stars, or in other words, why they show enhanced mass loss. WNL stars have similar effective temperatures and surface compositions as typical O-supergiants (see e.g. Crowther et al. 2002) but they show much stronger wind emission lines. To investigate their mass loss properties we have prepared a series of hydrodynamic PoWR models with typical WNL parameters (referring to Hamann et al. 2006). We adopt a high luminosity of $L_\star = 10^{6.3}\ L_\odot$, effective core temperatures in the range $T_\star = 33{-}55$ kK, a clumping factor of $D_{max} = 10$, and typical WN surface abundances with $X_H = 0.2$, $X_{He} = 0.78$, and $X_N = 0.014$ (for more details see Table 2, $T_\star$ grid). For our hydrodynamic models it is moreover necessary to prescribe the stellar mass. We study two values, $M_\star = 67\ M_\odot$ and $55\ M_\odot$, corresponding to relatively large Eddington factors $\Gamma_e = 0.55$ and 0.67 (note that we are giving here $\Gamma_e \equiv \chi_e L_\star/4\pi cGM_\star$ for a fully ionized plasma).

The obtained mass loss rates are plotted in Fig. 1. We find a strong dependence on Γ_e (or equivalently the L/M ratio), and on the stellar temperature ($\dot{M} \propto T_\star^{-3.5}$). Note that both effects mark an important change in the properties of WR-type winds, compared to the radiatively driven winds of OB stars. As we will discuss in more detail in Sect. 4.1, this is a direct consequence of the optically thick wind physics, where the location of the critical point is coupled to Γ_e and the local electron temperature T_e.

The synthetic spectra obtained from our calculations are consistent with observed WNL spectra. In Fig. 1 we have indicated four specific objects which are in good qualitative agreement with our models. They reflect the observed sequence of WNL spectral subtypes, starting with WN 6 at 55 kK to WN 9 at 31 kK. Note that these objects show similar line spectra as our models, but different luminosities and surface compositions. Because of this, their actual mass loss rates may differ from the values given in Fig. 1. A detailed comparison with the WN 7 subtype WR 22 is presented in the next section.

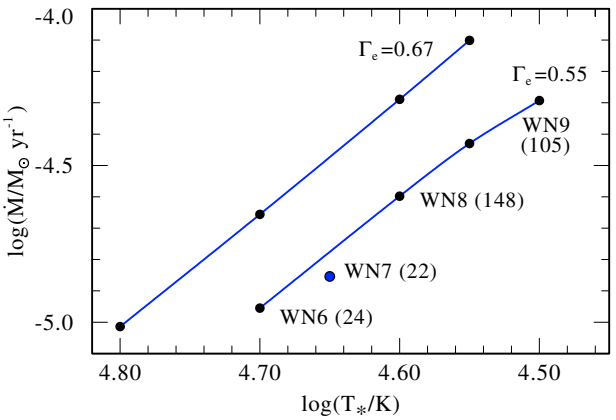

Fig. 1. Wind models for galactic WNL stars: mass loss rates for different stellar temperatures $T_\star$ and Eddington factors Γ_e. The corresponding spectral subtypes are indicated together with WR numbers of specific galactic objects (according to van der Hucht 2001, in brackets), which show a good agreement with the synthetic line spectra. Note that the models are computed for a fixed stellar luminosity of $10^{6.3}\ L_\odot$. The WN 7 model (WR 22) is slightly offset from the standard grid models because it is calculated with an enhanced hydrogen abundance (see Sect. 3.2).

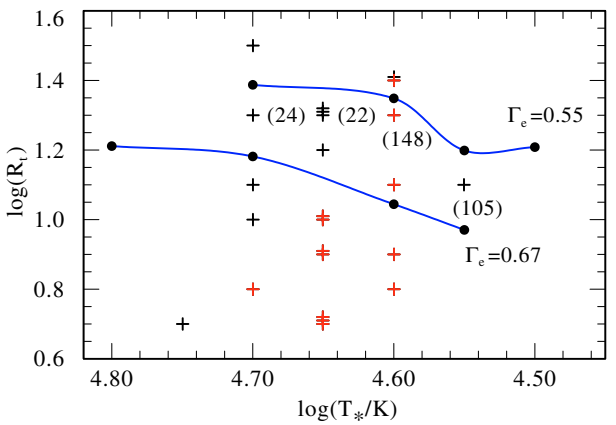

Fig. 2. Wind models for galactic WNL stars: wind densities compared to observed values according to Hamann et al. (2006). In the R_t–$T_\star$ plane, our models (solid curves) reproduce the *upper* part of the observed WNL sample (crosses), corresponding to WNL stars with *low* wind densities (see text for the definition of R_t). The objects belonging to the enigmatic class of WN 8 spectral subtypes are indicated in red.

For a more comprehensive overview we compare our results to the stellar parameters obtained by Hamann et al. (2006) for the galactic WNL sample. However, because our computations are restricted to a fixed luminosity, we cannot simply compare the obtained mass loss rates. We thus employ the transformed radius

$$R_t = R_\star \left[\frac{v_\infty}{2500\ \mathrm{km\,s^{-1}}} \Big/ \frac{\sqrt{D}\dot{M}}{10^{-4}\ M_\odot\ \mathrm{yr^{-1}}} \right]^{2/3}, \qquad (2)$$

which is a luminosity-independent measure of the wind density. As outlined by Hamann & Koesterke (1998a), models with the same R_t are scale invariant, i.e., for a given value of $T_\star$ and a given surface chemistry they show the same line equivalent widths. The results are shown in Fig. 2. In the R_t–$T_\star$ plane our wind models reproduce the upper half of the observed WNL sample, i.e., WNL stars with low wind densities. The large scattering in the observations makes it difficult to draw clear

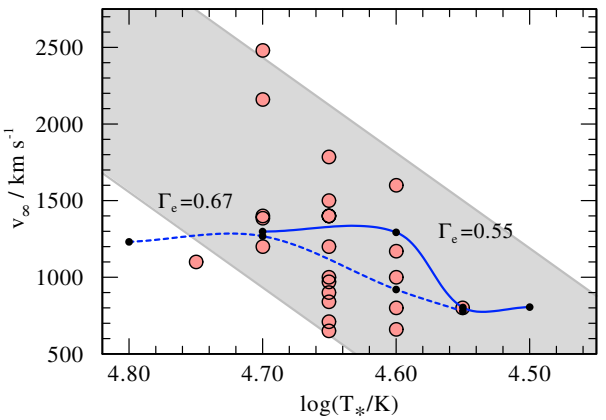

Fig. 3. Wind models for galactic WNL stars: terminal wind velocities compared to observed values taken from Hamann et al. (2006), and the observed trend with spectral subtype (from Niedzielski & Skorzynski 2002). Our models (solid curve for $\Gamma_e = 0.55$ and dashed curve for $\Gamma_e = 0.67$) reproduce the observed trend of increasing v_∞ with increasing $T_\star$, but they tend to underestimate the high values observed for the hottest objects.

conclusions from this comparison. Note, however, that e.g. constant mass loss rates would show a clear trend with $R_t \propto R_\star \propto T_\star^{-2}$. The fact that the observations as well as our models show no clear trend thus supports our finding of increasing $\dot{M}$ with decreasing $T_\star$. The large part of the high wind density objects, which are not reproduced by our models, belong to the enigmatic WN 8 subtypes. These stars show strong photometric variations. Pulsations thus might play a role in their mass loss (see the discussion in Sect. 5.4). Moreover, most of them are located far away from stellar clusters, i.e., their luminosities are largely unknown. They might thus belong to a different group of objects with much lower luminosities.

In Fig. 3 we compare the obtained terminal wind velocities with observations. The galactic WR stars are known to show a trend of increasing v_∞ for earlier spectral subtypes (Howarth & Schmutz 1992; Niedzielski & Skorzynski 2002). In Fig. 3 this trend is indicated by the grey shaded area, together with observed values for single WNL stars from Hamann et al. (2006). Our models reproduce approximately the mean of the observed values. However, although they show increasing v_∞ with increasing $T_\star$, this trend is less pronounced than the observed one. Particularly around $T_\star = 50$ kK our models tend to saturate whereas the observed values still increase. In Sect. 4.2 we will show that this issue might be related to the detailed radial dependence of the clumping factor $D(r)$.

3.2. Test case: WR 22

To verify our assumption of high L/M ratios for WNL stars we perform a more detailed comparison with WR 22, an eclipsing WR+O binary system in Carina OB 1, which is classified as WN 7h. WR 22 is an ideal target for our purposes because mass estimates are available for the WN component. Moreover, the O star component is so faint that at least 90% of the observed flux originates from the WR star, i.e., the WN spectrum is only marginally contaminated. From the radial velocity curve Schweickhardt et al. (1999) derived a mass of $M_{\rm WR} \sin^3 i = 55.3 \pm 7.3\ M_\odot$, whereas Rauw et al. (1996) obtained $71.7 \pm 2.4\ M_\odot$, both with $M_{\rm WR}/M_{\rm O} = 2.7$. The inconsistency is presumably due to the high eccentricity of the system, and the

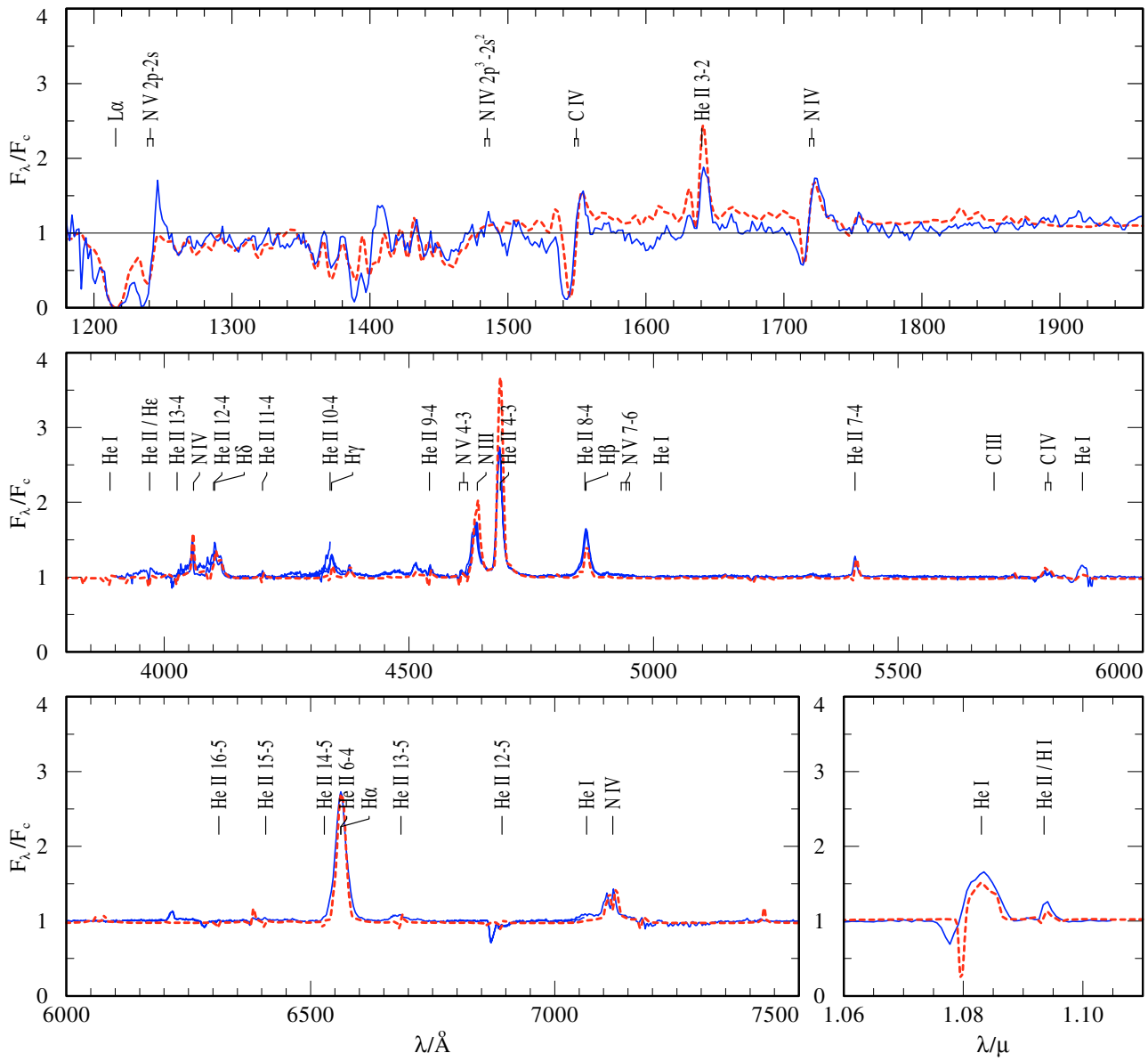

Fig. 4. WR 22: comparison of the synthetic spectrum from our hydrodynamic model (dashed line, red) with observations (blue). Fluxes are given in units of the model continuum flux. Note that *only* the optical and IR data are rectified by hand, whereas the observed UV fluxes are divided by the model continuum corrected for interstellar absorption and distance. The detailed model parameters are given in Table 2.

extremely high signal-to-noise ratio that is need to detect the O star absorption lines.

In Fig. 4 we compare our best fitting synthetic spectrum to observations of WR 22. The stellar parameters are the same as for our previous grid models, but with $T_\star = 44.7$ kK and $X_\mathrm{H} = 0.4$, as derived by Hamann et al. (2006). With our hydrodynamic models we obtain a good spectral fit for an Eddington parameter of $\Gamma_\mathrm{e} = 0.55$, corresponding to a mass of 78.1 $M_\odot$ (the detailed model parameters are summarized in Table 2). The resulting model reproduces the observed emission line spectrum reasonably well, although the terminal wind velocity appears too small and the He I lines are slightly too weak. Nevertheless, the fit quality is more than satisfactory for our present purposes. The absolute flux distribution of WR 22 (from IR to UV) is closely reproduced with a luminosity of $10^{6.3}$ $L_\odot$ for an adopted distance modulus of 12.1 mag (Lundström & Stenholm 1984), and an interstellar extinction law according to Fitzpatrick (1999) with $E_{B-V} = 0.42$ and $R = 3.6$ (see Fig. 5).

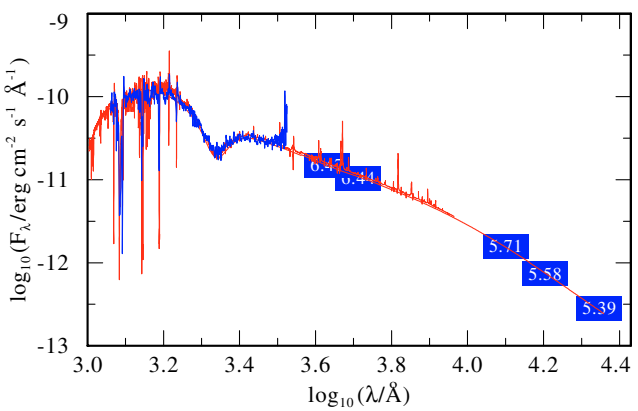

Fig. 5. WR 22: observed flux distribution in absolute units (blue), including optical + 2MASS IR photometry (blue boxes), compared with the model flux corrected for interstellar extinction (red). The detailed model parameters are given in Table 2.

The mass of 78.1 $M_\odot$, as obtained from our models, is apparently in good agreement with the mass estimate by Rauw et al. (1996). However, for a proper comparison we need to take into account the inclination of the system, its distance, and possiple uncertainties in our spectral analysis.

The inclination of the system is constrained by the detection of an eclipse near periastron, where the O star is obscured by the WR star (Gosset et al. 1991). According to Schweickhardt et al. (1999) the periastron angle of the O star is 88°, and the orbit is highly eccentric with $e = 0.598$. No eclipse is detected near apastron, presumably because of the eccentricity of the orbit (Gosset et al. 1991). According to our models the radius of the stellar disk, i.e., the radius where $\tau_{\rm Ross} = 2/3$, is only slightly larger than the stellar core radius: $R_{2/3} = 1.056\ R_\star = 25.0\ R_\odot$. Adopting $a \sin i = 2.31 \times 10^8$ km $= 13.3\ R_{2/3}$ from Schweickhardt et al. (1999), we obtain a projected distance between both stars of 5.35 $R_{2/3}$ at periastron and 21.3 $R_{2/3}$ at apastron. The eclipse detection at periastron thus constrains $\sin i$ to values above 0.983 ($\sin^3 i \geq 0.950$). The non-detection at apastron limits $\sin i$ to values below 0.9982 ($\sin^3 i \leq 0.9946$), i.e., $\sin^3 i = 0.972 \pm 0.022$. Note that we have neglected the size of the O star in this estimate because a significant part of the O star is obscured but it is not clear whether the eclipse is full or partial. Applying our limits for $\sin^3 i$ we obtain $M_{\rm WR} = 56.9 \pm 8.5\ M_\odot$ using the orbital data from Schweickhardt et al. (1999), and $M_{\rm WR} = 73.8 \pm 4.0\ M_\odot$ based on Rauw et al. (1996). Hence the inclination induces only small additional uncertainties in the mass estimate.

The emission line strengths computed in our models depend strongly on the wind density, and thus on the obtained mass loss rates. These are chiefly affected by $T_\star$ and $\Gamma_{\rm e}$. While $T_\star$ can be reliably determined from spectral line diagnostics, $\Gamma_{\rm e}$ depends on the L/M ratio and on the hydrogen abundance $X_{\rm H}$. Again, $X_{\rm H}$ can be determined from spectral line ratios. Our models thus constrain the L/M ratio, with an error of about 10% (see Sect. 4.2 for a discussion of additional systematic errors). The obtained value for $M_\star$ thus scales with $L_\star$, which depends on the adopted distance and interstellar extinction. The extinction is determined within our spectral analysis from the continuum shape in the UV. Together with $T_\star$ this might introduce an additional error of about 10% in $L_\star$. More critical is the adopted distance modulus for Carina OB1. Values in the literature span a range between 11.8 mag (Davidson et al. 2001) and 12.55 mag (Massey & Johnson 1993), corresponding to an uncertainty of a factor of two in $L_\star$. The unknown distance of the system is thus the main source of uncertainty in our analysis.

We have seen that, with an intermediate distance modulus of 12.1 mag (according to Lundström & Stenholm 1984), our model is in agreement with the mass determination by Rauw et al. (1996). For the low value of 11.8 mag, WR 22 would become slightly fainter ($10^{6.18}\ L_\odot$) and our mass estimate would roughly scale down to 59 $M_\odot$, now in agreement with Schweickhardt et al. (1999). With 12.55 mag we would obtain a very high luminosity of $10^{6.5}\ L_\odot$ which puts WR 22 extremely close to the Eddington limit or even above ($\Gamma_{\rm e} = 0.92$ for 74 $M_\odot$, and $\Gamma_{\rm e} = 1.24$ for 55 $M_\odot$). Note that in view of the additional $b-b$ and $b-f$ contributions to the mean opacity also $\Gamma_{\rm e} = 0.7$ would imply a super-Eddington luminosity (see Sect. 4.2). Such a large distance to WR 22 thus seems to be very problematic.

At the present stage we conclude that WR 22 has a very high luminosity of the order of $10^{6.3}\ L_\odot$, and that it is located rather close to the Eddington limit. Chiefly because of the uncertain distance, the possible error in the luminosity is large. Nevertheless, mass estimates from radial velocity measurements support our assumption of large Eddington factors for WNL subtypes. With the large distance determined by Massey & Johnson (1993), WR 22 would even exceed the Eddington limit.

3.3. Grid calculations for different metallicities

The wind acceleration in our models predominantly originates from Fe line opacities. We thus expect a strong dependence of the mass loss on metallicity. To investigate this dependence we have prepared a grid of hydrodynamic WNL models for a wide range of Z. Because we already know about the fundamental importance of the Eddington limit for WR-type winds we have introduced $\Gamma_{\rm e}$ as an additional free parameter. The stellar core parameters ($L_\star$, $T_\star$, $R_\star$), and the surface abundances $X_{\rm H}$ and $X_{\rm He}$ are adopted from our WR 22 model in the previous section. $M_\star$ is adjusted to match the desired values of $\Gamma_{\rm e}$, and Z is varied by scaling the surface mass fractions $X_{\rm C}$, $X_{\rm N}$, $X_{\rm O}$, $X_{\rm Si}$, and $X_{\rm Fe}$ (see Table 2, Grid 2).

The results are presented in Fig. 6. The solid (blue) curves indicate model series for different *initial* metallicities, i.e., with CNO abundances corresponding to a secondary helium and nitrogen enrichment by the CNO-process. As expected, the models show a strong Z-dependence. However, our second free parameter $\Gamma_{\rm e}$ turns out to be at least equally important. In fact it seems that the proximity to the Eddington limit is the primary reason for the enhanced mass loss of WR stars. Remarkably, the high WR-type mass loss rates can even be maintained for very low Z, if the stars are close enough to the Eddington limit.

The dashed (red) curve in Fig. 6 indicates models with $X_{\rm Fe} = 0$ and $X_{\rm Si} = 0$ but $X_{\rm CNO} = Z_\odot$ (see Table 2, Grid 3). These models show to what extent the *primary* production of nitrogen may affect the mass loss at different metallicities. Such an enhancement is expected for fast rotating stars at extremely low metallicities (see Meynet et al. 2006). Interestingly, these models show a similar behavior to the Fe-rich models. The solar-like CNO mass fraction produces a stellar wind that is similar to an Fe-rich model with $1/50\ Z_\odot$. This means that the potential mixing of primary nitrogen to the surfaces of metal-poor stars considerably affects the expected mass loss rates.

In the bottom panel of Fig. 6 we show the terminal wind velocities obtained from our models. First, the models clearly predict decreasing wind velocities with decreasing Z. This finding is in agreement with observations although the observational evidence is not as clear as our prediction (see e.g. Conti et al. 1989; Crowther 2000). Second, the terminal velocities tend to stay constant or even increase with $\dot{M}$. This behaviour again indicates important qualitative differences to OB star winds. For OB stars the well-established wind momentum-luminosity relation predicts the opposite behaviour, i.e., decreasing wind velocities for increasing mass loss (Kudritzki et al. 1999). A closer inspection of our models shows that the changes in the velocity structure are related to changes in the wind ionization. For cases where an increase of $\dot{M}$ leads to recombination of Fe, the velocity increases in the recombination region due to the newly exposed line opacities. Models with a similar ionization structure, on the other hand, show similar wind velocities. Note that our assumption of a constant Doppler broadening ($v_{\rm D} = 100$ km s^{-1}, see Sect. 2.2) might affect the results for extremely low Z, because for these cases the wind velocities are of the same order of magnitude as $v_{\rm D}$.

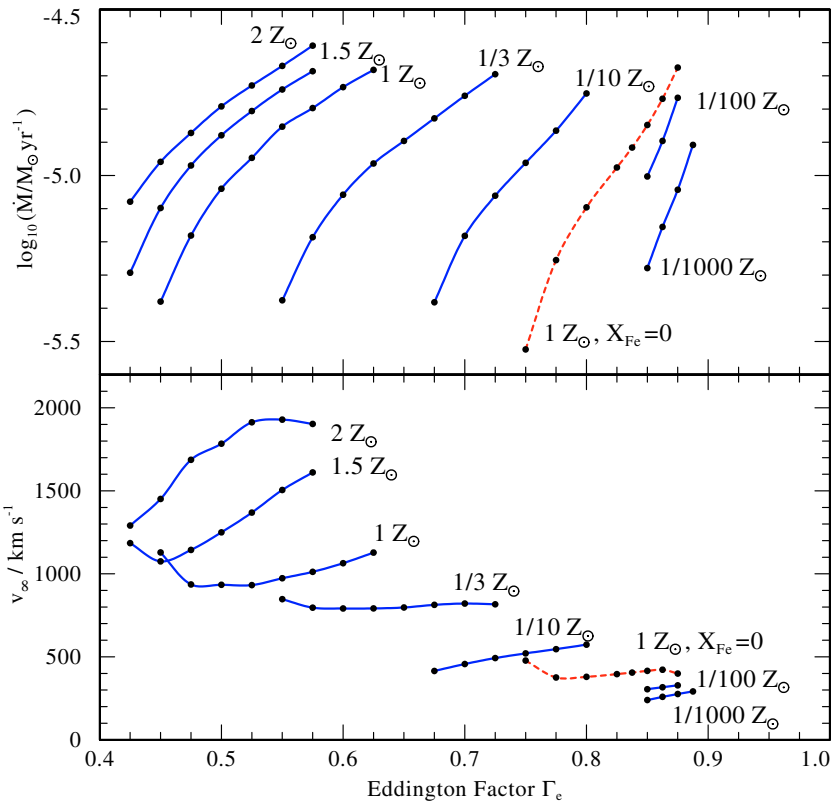

Fig. 6. WNL star mass loss in the range from $Z_\odot/1000$ to 2 $Z_\odot$: mass loss rates (*top*) and terminal wind velocities (*bottom*), as obtained from our hydrodynamic grid models, are plotted vs. the Eddington factor Γ_e (the models are computed for a fixed value of $L_\star = 10^{6.3}\ L_\odot$, the variation of Γ_e thus effectively corresponds to a variation of the stellar mass). Model parameters are given in Table 2. The solid blue lines indicate model series where Γ_e is varied for a given value of Z. Note that strong WR-type mass loss occurs over the whole range of Z, if Γ_e approaches unity. Moreover, the models show a clear trend of decreasing v_∞ with decreasing Z. The dashed red lines indicate models with zero Fe, but solar-like CNO abundance. They show that strong WR-type mass loss is also possible for extremely metal-poor stars due to the self-enrichment with primary nitrogen.

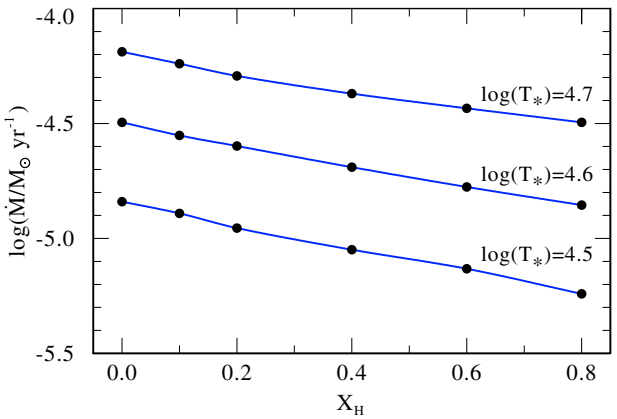

Fig. 7. The dependence of WNL star mass loss on the hydrogen abundance X_H: for otherwise fixed stellar parameters the mass loss depends only weakly on X_H, with $\dot{M} \propto {X_H}^{0.45}$. Model computations for three different values of $T_\star$ and fixed values of $\Gamma_e = 0.55$ and $L_\star = 10^{6.3}\ L_\odot$ are shown. Note that the stellar mass is varied to keep Γ_e constant.

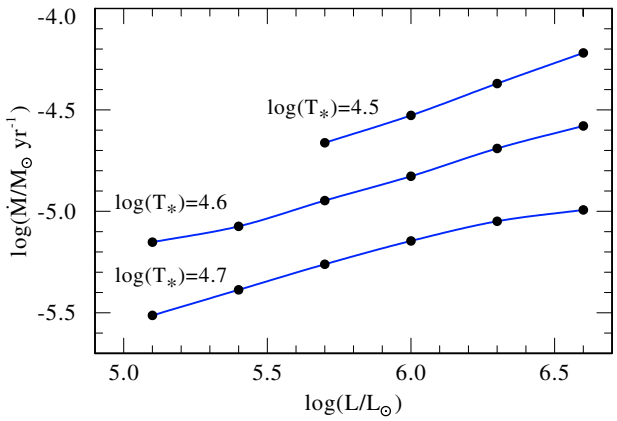

Fig. 8. The dependence of WNL star mass loss on luminosity: for otherwise fixed stellar parameters the mass loss depends relatively weakly on $L_\star$, with $\dot{M} \propto L_\star^{0.42}$. Model computations for three different values of $T_\star$ are shown. Note that the Eddington factor is fixed to $\Gamma_e = 0.55$ by keeping the L/M ration constant.

3.4. A mass loss recipe for WNL stars

A primary goal of our present work is to provide a recipe that describes the mass loss of WNL stars, dependent on the fundamental stellar parameters $M_\star$, $T_\star$, $L_\star$ and the surface mass fractions X_H, X_{He}, and Z. In the preceding sections we emphasized that, for fixed $L_\star$, the mass loss is chiefly determined by the proximity to the Eddington limit, i.e., by the Eddington factor Γ_e. We thus expect that the main influence of the surface mass fractions X_H and X_{He} is due to the number of free electrons, which enters the Eddington parameter for a fully ionized plasma in the form $\Gamma_e = 10^{-4.813}(1 + X_H)\, L_\star/M_\star$. In Fig. 7 we show that for fixed Γ_e the influence of the light elements is indeed only moderate, with $\log(\dot{M}) \propto -0.45\, X_H$. As we will discuss in Sect. 4.3, the slight decrease of $\dot{M}$ with increasing hydrogen abundance is due to the influence of the He II continuum in the critical layers.

We present in Fig. 8 a series of models with varied $L_\star$. Again, the stellar parameters are adopted from WR 22. Γ_e is fixed to a value of 0.55, and $L_\star$ and $T_\star$ are varied over the relevant parameter range (see Table 2). Notably, the resultant mass loss rates depend only weakly on $L_\star$, with $\dot{M} \propto L_\star^{0.42}$. Note that this again denotes an important difference to OB star winds for which a much stronger dependence is expected (see the discussion in Sect. 4.1).

We combine our results in the following form. For the dependence on $T_\star$ we use the scaling relation from Sect. 3.1 with $\dot{M} \propto T_\star^{-3.5}$, and for the dependence on X_H and $L_\star$ we use $\dot{M} \propto {X_H}^{0.45} L_\star^{0.42}$ from this section. For the coupled dependence on Γ_e and Z from Sect. 3.3 we use a more complex description

of the form $\dot{M} \propto (\Gamma_e - \Gamma_0)^\beta$, where the Z-dependent parameters $\Gamma_0(Z)$ and $\beta(Z)$ are determined by a multi-dimensional fit procedure. The resultant mass loss recipe is in good agreement with our grid computations in Fig. 6, with an accuracy better than 0.05 dex except for two data points with a maximum deviation of 0.1 dex. Combining all these relations, we arrive at a mass loss recipe of the form

$$\begin{aligned}\log\left(\dot{M}_{\rm WNL}/\,M_\odot\,{\rm yr}^{-1}\right) &= -3.763\\ &+\beta\cdot\log\left(\Gamma_e-\Gamma_0\right)-3.5\cdot\left(\log(T_\star/{\rm K})-4.65\right)\\ &+0.42\cdot\left(\log(L_\star/L_\odot)-6.3\right)-0.45\cdot\left(X_{\rm H}-0.4\right),\end{aligned}\tag{3}$$

or

$$\begin{aligned}\log\left(\dot{M}_{\rm WNL}/\,M_\odot\,{\rm yr}^{-1}\right) &= 10.046\\ &+\beta\cdot\log\left(\Gamma_e-\Gamma_0\right)-3.5\log(T_\star/{\rm K})\\ &+0.42\log(L_\star/L_\odot)-0.45\,X_{\rm H},\end{aligned}\tag{4}$$

with

$$\beta(Z) = 1.727 + 0.250\cdot\log(Z/Z_\odot),\tag{5}$$

$$\Gamma_0(Z) = 0.326 - 0.301\cdot\log(Z/Z_\odot) - 0.045\cdot\log(Z/Z_\odot)^2.\tag{6}$$

This recipe is only valid for optically thick winds that are driven by the cool Fe opacity-peak. It is thus only applicable in a limited range of stellar temperatures. $T_\star$ should never exceed a value of ≈70 kK because then the opacity minimum between the hot and the cool Fe-peaks is reached. On the cool side, for $T_\star < 30$ kK, our models reach a limit where the radiative force exceeds gravity in the deep hydrostatic layers due to the hot Fe-peak. At this point the region of LBV-type instabilities might be reached (see the discussion in Sect. 5.4).

According to Eqs. (3) and (4) the WNL mass loss rates would go to zero when Γ_e approaches Γ_0. Our recipe of course loses validity before this point, when the winds become optically thin. For our present grid models this happens at a mass loss rate of $\log(\dot{M}/\,M_\odot\,{\rm yr}^{-1}) \approx -5.5$ when $\Gamma_e - \Gamma_0 \approx 0.1$. Note that this criterion should roughly depend on the wind density at the sonic point. We thus expect the limiting mass loss rate, above which our models are valid, to be of the order of $\log(\dot{M}_{\rm lim}/\,M_\odot\,{\rm yr}^{-1}) \approx -5.5 + 2\log(R_\star/23.7\,R_\odot)$. Note that Eqs. (5) and (6) which describe our parameters $\Gamma_0(z)$ and $\beta(z)$ are strictly limited to the investigated parameter range of $2\,Z_\odot < Z < 10^{-3}\,Z_\odot$.

4. The properties of WR-type stellar winds

In the present section we discuss the properties of WR-type stellar winds as opposed to the thin winds of OB stars (Sect. 4.1). In this context we discuss possible error sources, with emphasis on the unknown turbulent velocities and wind clumping factors (Sect. 4.2). Moreover, we compare our results with other mass loss predictions for WR and OB stars (Sect. 4.3).

4.1. Optically thick stellar winds

In Sects. 3.1 and 3.4 we have seen that our WR wind models are qualitatively different from OB-type stellar winds. In particular we find a strong dependence on the Eddington factor Γ_e, a steep increase of $\dot{M}$ with decreasing effective temperature ($\dot{M} \propto T_\star^{-3.5}$), and a weak dependence on the stellar luminosity ($\dot{M} \propto L_\star^{0.4}$). Our results from Sect. 3.3 even suggest a violation of the wind momentum-luminosity relation, which is extremely well-established for OB star winds (see, e.g., Kudritzki et al. 1999; Mokiem et al. 2005, 2007b). Instead, the velocity structure in our models seems to be dominated by ionization effects.

Within the classical CAK theory for OB star winds (Castor et al. 1975) a mass loss relation of the form $\dot{M} \propto M_{\rm eff}^{(\alpha-1)/\alpha} L_\star^{1/\alpha}$ is expected. As explained in Sect. 2.1, the parameter α characterizes the response of the radiative acceleration to the velocity gradient, and typically lies around $\alpha \approx 0.6$. $M_{\rm eff}$ denotes the effective stellar mass, reduced by the contribution of the radiative acceleration on free electrons $M_{\rm eff} = M_\star(1-\Gamma_e)$. In contrast to our WR models, the expected dependence on the stellar mass is thus rather weak, while the luminosity dependence is comparatively strong. Moreover, OB star winds do not have a pronounced wind ionization structure, apart from a sudden change in ionization around spectral type B1 (the bistability jump, see Lamers et al. 1995). The ionization thus only plays a minor role in the wind dynamics and is usually expressed by a small correction to the α parameter (see Abbott 1982).

As outlined in Sect. 2.1, the α parameter is determined numerically within our models and enters the hydrodynamic solution scheme as a depth-dependent quantity. Compared with the typical values for OB stars ($\alpha \approx 0.6$) our present models show remarkably low values ($\alpha \approx 0.2$). This result is in line with our previous finding of $\alpha \approx 0$ for the extremely thick winds of WC stars (Gräfener & Hamann 2005, see also the discussion therein). It seems that $\alpha \to 0$ for thick winds. Such a behaviour is expected for the deep atmospheric layers, where the diffusion approximation is applicable. For the outer wind such low values again indicate important qualitative differences to "classical" line-driven winds. At the present stage we attribute this effect to two mechanisms, which are expected for the case of WR-type winds, and which are both detectable in our models: the dominance of weak spectral lines, and massive line overlap.

First, the high density of WR winds leads to an overpopulation of excited energy levels by recombination cascades. This results in an increase of the number of optically thin lines. Note that α also reflects the relative contribution of optically thick spectral lines to the overall wind driving (see, e.g. Puls et al. 2000). A dominance of optically thin lines thus leads to a decrease of α, or in other words to the formation of a pseudo-continuum of thin lines. Second, the resulting ionization structure leads to non-local line overlaps. In such a situation it can happen that an additional Doppler-shift causes a reduction of the radiative force because of the increased line-shadowing. Both effects result in a dominance of ionization effects over the usual CAK wind physics, as is observed in our models.

Alternative theories for optically thick stellar winds have been proposed by Pistinner & Eichler (1995) and Nugis & Lamers (2002). Both works assume that the conditions at the critical point depend on the Rosseland mean opacity, and they show that the observed mass loss rates of WR stars are in agreement with this assumption. In the following we will show that the scaling relations obtained from our present models can be understood within this framework. They reflect the dominant role of the wind optical depth for WR-type mass loss, which we identify as the basic reason for the qualitative differences to OB star winds. Note, however, that the conditions within our models do not strictly reflect the limit of optically thick winds. Our present WNL models show only moderate optical depths, so that their mass loss actually reflects a case in between the optically thick and the optically thin limit.

The basic assumption of the optically thick wind approach is that the radiation field at the critical point of the wind flow can be described in the diffusion limit (see Nugis & Lamers 2002). It follows that 1) the sonic point becomes the critical point of the equation of motion $v_c = a(T_c)$, 2) a specific (critical) value of the Rosseland mean opacity must be reached at the sonic point

$\chi_c = 4\pi cGM_\star/L_\star$, and 3) the mass loss rate is connected to the density and the temperature at this point via the equation of continuity $\dot{M} = 4\pi R_\star^2 \rho_c v_c$.

The importance of the L/M ratio for this kind of mass loss follows directly from condition 2), which means that the radiative acceleration just balances the gravitational attraction at the critical point. For the formation of an optically thick wind it is thus mandatory that the L/M ratio and χ_c are large enough, i.e., the star must be close to the Eddington limit and the mean opacity at the critical point must be large. Furthermore, the mean opacity must increase outward to obtain an outward-directed net acceleration above the critical point. These conditions restrict the temperature T_c at the critical point to limited temperature ranges connected to the occurrence of the two Fe opacity-peaks. With $T_c = 30{-}45$ kK our present WNL models are driven by the cool Fe-peak opacities. Our previous WCE model with $T_c = 199$ kK, on the other hand, clearly belonged to the regime of the hot Fe-peak (see Gräfener & Hamann 2005).

The necessity to reach certain values of T_c marks a basic change of paradigm with respect to OB star winds. The temperature at large optical depth scales as $T^4 \propto T_\star^4 \tau$. Hence large wind optical depths τ_c are needed to reach large values of T_c. For our case, where a specific temperature T_c must be reached at τ_c this means that $\tau_c \propto T_\star^{-4}$.

We found a very strong dependence on $T_\star$ for our models with fixed Γ_e in Sect. 3.1. This behaviour is related to the scaling properties of τ_c. If we assume that τ_c scales with ρ_c and the density scale height H, we get $\tau_c \propto \rho_c H \propto \rho_c R_\star^2/M_{\rm eff} \propto \rho_c R_\star^2/M$. From this it follows directly that $\tau_c \propto \dot{M}/M$ because $\dot{M} = 4\pi R_\star^2 \rho_c v_c \propto R_\star^2 \rho_c$, for the given value of $v_c = a(T_c)$. Finally we get $T_\star^{-4} \propto \tau_c \propto \dot{M}/M$, or $\dot{M} \propto T_\star^{-4} L$ for fixed L/M.

This scaling relation indeed predicts a strong dependence on $T_\star$ and a relatively weak dependence on L for optically thick winds. It is caused by the scaling properties of τ_c with the density scale height H, and the requirement that a certain temperature regime is reached at the critical point. The formation of optically thick winds is thus strongly related to the extension of the deep atmospheric layers (i.e., the increase of H) close to the Eddington limit.

With $\dot{M} \propto T_\star^{-3.5} L^{0.4}$ our computational models show a similar dependence on $T_\star$ and an even weaker dependence on L. The differences are presumably due to the idealized assumptions in our analytic derivation. Nevertheless, we conclude that our models show a qualitative behaviour that is very different from OB star winds, but can be understood in the framework of the optically thick wind approach. Note that the specific properties of optically thick stellar winds originate from the deep atmospheric layers, and that an exact modelling of these layers is required to obtain qualitatively correct results.

4.2. The influence of wind clumping and micro-turbulence

Apart from the work by Schmutz (1997), the influence of wind clumping has been largely ignored in previous studies of radiatively driven winds. In our own work we have demonstrated that clumping increases the radiative acceleration in O supergiant (Gräfener et al. 2002; Gräfener & Hamann 2003) and WR star winds (Gräfener & Hamann 2005). The specific choice of the clumping factor $D(r)$ thus has an influence on our results. In Sect. 2.2 we have described how $D(r)$ is parametrized within our models. This parametrization is based on observational grounds. Clumping diagnostics are however very rough and restricted to the formation region of the diagnostic features. In principle, $D(r)$ thus could be varied in a certain range. In the present section we discuss to what extent this would affect our results. In addition, we investigate the influence of the Doppler broadening velocity v_D. In our models v_D is usually set to a fixed, highly supersonic value of $v_D = 100$ km s^{-1}. This choice is motivated by the observed broadening velocities in P-Cygni type line profiles (e.g. Hamann 1981), and by the fact that our CMF radiative transfer is limited to relatively large values of v_D (see Sect. 2.2). Again, we have a certain freedom in the choice of v_D and we want to quantify its influence on our results.

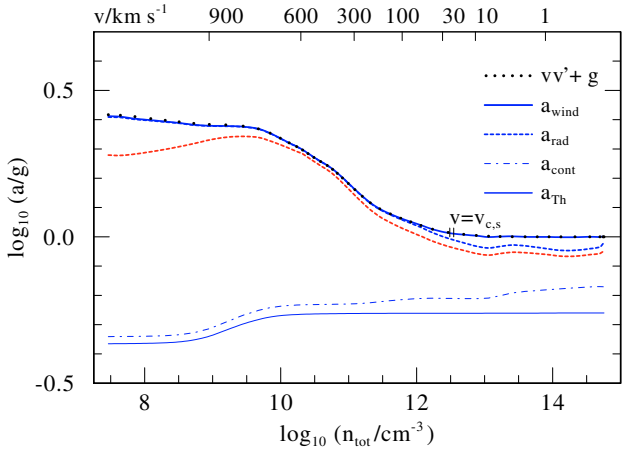

Fig. 9. WR 22: wind acceleration in units of the local gravity g. The total atomic density is given as depth index. The blue curves indicate the acceleration within our WR 22 model from Sect. 3.2. Indicated are the radiative acceleration on free electrons ($a_{\rm Th}$), on continua ($a_{\rm cont}$), the total radiative acceleration including lines ($a_{\rm rad}$), and the total wind acceleration including the pressure term ($a_{\rm wind}$). The red line indicates the radiative acceleration within our test model with a reduced Doppler broadening velocity $v_D = 50$ km s^{-1}.

We start with Fig. 9 where we show the wind acceleration within our model for WR 22. In this logarithmic diagram we plot the wind acceleration $a_{\rm wind}$ in units of the local gravity g, vs. the total atomic number density $n_{\rm tot}$ as depth index. The plot covers the whole model atmosphere from the hydrostatic layers where $\log(a_{\rm wind}/g) = 0$, through the critical point, to the outer boundary at $r = 1000\,R_\odot$. The critical point (with $v_c = 23.3$ km s^{-1}) and the sonic point (with $v_s = 20.8$ km s^{-1}) are both located very close together at the point where $a_{\rm rad} \approx g$, in agreement with our condition 2) from the previous section. In the hydrostatic layers below the sonic point (at densities above $\log(n_{\rm tot}/{\rm cm}^{-3}) \approx 12.5$), the radiative acceleration $a_{\rm rad}$ (indicated by the dashed blue line) lies only slightly below g, with $\log(a_{\rm rad}/g) \approx -0.05$. This shows that, although with $\Gamma_e = 0.55$ we are still away from the Eddington limit, our model atmosphere is in fact rather close to instability (with a "true" Eddington parameter, including all opacity sources, of $\Gamma \approx 0.9$).

Being a late spectral subtype, WR 22 is in a temperature regime where the cool Fe-peak opacities dominate. In Fig. 9, however, we can see that close to the critical point ≈70% of the radiative force is due to continua. Nevertheless, the Fe line opacities play the dominant role in determining the mass loss because they are responsible for the *increase* of $a_{\rm rad}$ which finally leads to the crossing of the Eddington limit at the critical point. The fact that the line contribution in the deep layers is so small compared to continua (which are dominated by Thomson scattering) indicates that mostly weak lines are responsible for the radiative driving, i.e., the sub-critical layers are supported by a pseudo-continuum of millions of weak Fe-group transitions.

Table 3. Model parameters and resulting wind parameters for our test models from Sect. 4.2, compared to the WR 22 model from Sect. 3.2. For models v_{D1} and v_{D2} the Doppler broadening velocity has been reduced to $v_D = 50$ km s^{-1}. For models $D1$ and $D2$ the wind clumping has been increased by a factor of four.

Model	WR 22	v_{D1}	v_{D2}	$D1$	$D2$
$M_\star/M_\odot$	78.1	78.1	73.5	78.1	78.1
Γ_e	0.55	0.55	0.585	0.55	0.55
v_D/ km s^{-1}	100	50	50	100	100
D_{max}	10	10	10	40	40
τ_1	0.7	0.7	0.7	0.7	0.7
τ_2	0.35	0.35	0.35	0.35	0.175
$\dot{M}/ M_\odot$ yr^{-1}	$10^{-4.85}$	$10^{-4.99}$	$10^{-4.87}$	$10^{-4.61}$	$10^{-4.80}$
v_∞/ km s^{-1}	974	932	938	1859	1764
$R_t/R_\odot$	21.7	25.9	21.7	14.5	18.6
η	0.34	0.23	0.31	1.12	0.69

From Fig. 9 it also becomes clear why our models are extremely sensitive to changes of a_{rad} close to the critical point. The dashed red line indicates the radiative acceleration within a model with exactly the same atmospheric structure but with a reduced broadening velocity of $v_D = 50$ km s^{-1}. This causes a rather small reduction of a_{rad} (by roughly −0.025 dex) in the deep atmospheric layers. In the outer wind region the relative effect is somewhat larger (−0.1 dex), the absolute wind velocity is however hardly affected because the wind is already close to its terminal speed. Although the effects in the deep layers are small it is obvious that even this small reduction of a_{rad} might cause a significant shift of the critical point towards smaller densities (i.e., smaller $\dot{M}$). A corresponding adjustment of $M_\star$, however, brings the star back to the same distance from the Eddington limit, and should thus restore the previous value of $\dot{M}$.

Test computations indeed confirm this behaviour. In Table 3 we compare our WR 22 model with full hydrodynamic models for which v_D has been reduced. For model v_{D1} all parameters apart from v_D are kept fixed, and $\dot{M}$ is indeed reduced by 0.24 dex. For model v_{D2} we have compensated this effect by a reduction of the stellar mass (0.026 dex) which indeed brings the star back to the previous state. Our results do depend on the assumed microphysics, because the location of the critical point strongly depends on the ratio a_{rad}/g in the deep atmospheric layers. For the same reason our predicted mass loss rates depend strongly on the Eddington factor Γ_e. The relatively large value of $v_D = 100$ km s^{-1} that we have chosen for our computations might thus have a significant effect on $\dot{M}$. However, it only causes a systematic shift of our results towards lower stellar masses, by ∼5%. Because the actual conditions in the sub-photospheric layers of WR stars are unknown, it is difficult to say if our assumption is correct.

The influence of wind clumping turns out to be even more important. In the last two columns of Table 3 we summarize the results of two test computations where the maximum clumping factor D_{max} has been scaled up by a factor of 4. Note that the spectroscopic properties of WR stars are determined by the product $\dot{M}\sqrt{D}$ (for details, see Hamann & Koesterke 1998a). An increase of the clumping factor by a factor of four thus approximately mimics the opacity of a wind with two times higher density. Consequently, a_{rad} also should scale with $\sqrt{D}$. Note that such a scaling relation is only expected to hold strictly for the populations of excited energy levels which are dominated by recombination processes.

Our test computations (models $D1$ and $D2$ in Table 3) show that the expected scaling of $a_{rad} \propto \sqrt{D}$ is fulfilled with an astonishing precision. Both test models with $D_{max} = 40$ show nearly exactly twice the terminal wind speed as our $D_{max} = 10$ models. Again, this is a hint that weak line transitions from excited (recombination-dominated) levels play a major role in the wind driving of WR stars. Moreover, the radial dependence of the wind clumping is also important. With our standard prescription of a τ-dependent clumping factor D, which rises from $D = 1$ to D_{max} between Rosseland optical depth $\tau_1 = 0.7$ and $\tau_2 = 0.35$ (see Sect. 2.2), the increase of D_{max} also leads to a significant increase of $\dot{M}$ (model $D1$ in Table 3). The reason for this is that in our prescription of $D(\tau)$ the wind clumping already sets in below the critical point, and thus affects the critical condition. For model $D2$ we have set τ_2 to a value of 0.175. In this way we have modified the growth rate of $D(r)$ such that the conditions at the critical point are similar to our WR 22 model. Again, the mass loss reacts very sensitively to the change of $D(r)$ and returns to the same value as the WR 22 model.

We conclude that different assumptions in the microphysics of our models may indeed cause significant changes in the predicted mass loss rates, if the region around the critical point is affected. However, these effects can always be compensated by a slight re-adjustment of the prescribed stellar mass. For the wind clumping we find that a_{rad} scales with $\sqrt{D}$. An increase of D in the outer wind layers only leads to an increase of the terminal wind speed by a factor $\sqrt{D}$. The possible discrepancies of our predicted wind speeds with observations (Sect. 3.3) thus might be resolved by a strong increase of $D(r)$ in the outer wind.

4.3. Comparison with other mass loss predictions

In the last few years an impressive agreement between theoretical mass loss predictions for OB stars and observations has been achieved (but see the discussion in Sect. 5.3). On the theoretical side, models by Vink et al. (2000, 2001), Pauldrach et al. (2001), and Krtička & Kubát (2004) agree well. Observationally, these results are confirmed on a large scale by the VLT-FLAMES survey of massive stars (Mokiem et al. 2005, 2007a). For the Z-dependence an exponential relation of the form $\dot{M} \propto Z^\gamma$ is generally accepted. Vink et al. (2001) find an exponent of $\gamma \approx 0.85$ for a broad range of OB star parameters. Note that this exponent is only valid if v_∞ is kept fixed. It thus needs to be corrected for the dependence of $v_\infty(Z)$, resulting in a relation of the form $\dot{M} \propto Z^{0.69}$ (Vink et al. 2001).

For WR stars the situation is less clear because only a few models are available. For late spectral subtypes Vink & de Koter (2005) recently claimed a similar Z-dependence as for OB stars, with $\gamma = 0.86$. As discussed previously, our present WNL models show a qualitatively different behaviour. Apart from the influence of clumping, micro-turbulence, and high wind density, it seems that models using a detailed CMF radiative transfer give results different from wind models based on the Sobolev approximation. Without wind clumping both available CMF codes (CMFGEN by Hillier & Miller (1998) and our own PoWR code) tend to predict very low wind accelerations a_{rad}. The models can only account for the observed wind momenta if clumping factors of the order of $D = 10$ or larger are assumed (Gräfener et al. 2000; Gräfener et al. 2002; Gräfener & Hamann 2005; Herald et al. 2001; Hillier 2003; Hillier et al. 2003). The reason for this is not yet fully understood (but see the discussion in Hillier et al. 2003). In the following we try to quantify these differences by a detailed comparison with previous works.

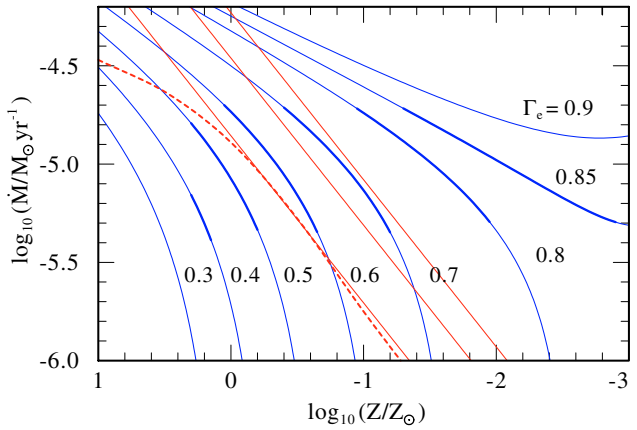

Fig. 10. The Z-dependence of WNL star mass loss: comparison of different mass loss predictions. The solid blue lines indicate the Z-dependent mass loss rates according to Eqs. (4)–(6) for fixed values of $\Gamma_e = 0.3$–0.9 (note that only the thick parts of the blue curves are in the region where grid models have actually been computed). They are compared to the mass loss predictions by Vink et al. (2001, solid red lines) for $\Gamma_e = 0.3$, 0.6, and 0.9, and the mass loss relation for WNL stars by Vink & de Koter (2005, dashed red line), which was obtained with $\Gamma_e = 0.34$.

For comparison we use the Z-dependent mass loss prescription for OB stars by Vink et al. (2001), and the WNL models by Vink & de Koter (2005). Note that, although the modeling of WNL subtypes was not particularly intended by Vink et al., their model grid partly overlaps with our present computations. In Fig. 10 we have extracted the Z-dependence of our WNL models from Eqs. (3)–(6), for fixed values of Γ_e. The blue curves indicate our results for Eddington parameters Γ_e = 0.3 to 0.9 (note that only the bold parts of the curves belong to the parameter range where models have actually been computed). The stellar parameters are fixed to $\log(T_\star/\mathrm{K}) = 4.65$, $\log(L_\star/L_\odot) = 6.3$, and $X_\mathrm{H} = 0.4$. The red solid lines indicate the mass loss predictions for OB stars by Vink et al. (2001) for the same stellar parameters and the same range of Eddington factors. The dashed red curve represents the WNL models by Vink & de Koter (2005), for slightly different stellar parameters (see below).

The OB star models by Vink et al. (2001) have a strictly exponential Z-dependence. Although Γ_e spans the same parameter range as our WNL models, the resulting mass loss rates cover a much narrower range, i.e., the dependence on Γ_e is much weaker. For large Eddington factors we obtain much higher mass loss rates, and a flatter decline with Z. These important differences are most likely caused by the different treatment of the wind dynamics in both codes. Vink et al. prescribe the velocity structure in their models and solve for a global consistency of the wind energy. The peculiar wind physics in the deep layers of WR winds, as described in Sect. 4.1, is not considered in such an approach.

The WNL models by Vink & de Koter (2005) are indicated by the red dashed line in Fig. 10. They are computed for a similar effective temperature as our models ($\log(T_\star/\mathrm{K}) = 4.60$), but for a lower hydrogen surface abundance ($X_\mathrm{H} = 0.15$), and a much lower luminosity ($\log(L_\star/L_\odot) = 5.62$). The stellar mass is fixed to 20 $M_\odot$, corresponding to $\Gamma_e = 0.37$, and the terminal wind speed is set to 840 km s^{-1}. For $Z < Z_\odot$ these models show exactly the same Z-dependence as their OB star counterparts, while for $Z > Z_\odot$ the mass loss tends to saturate. Moreover, Vink & de Koter detect a flattening of the Z-dependence for $Z < 10^{-4}\ Z_\odot$, which is beyond the parameter range investigated here.

For $Z_\odot > Z > 10^{-4}\ Z_\odot$ the WNL models by Vink & de Koter (2005) are in exact agreement with the mass loss prescription for OB stars by Vink et al. (2001). Note that Vink et al. (2001) assume a ratio of $v_\infty/v_\mathrm{esc} = 2.6$ for OB stars. With a typical stellar mass of 43.5 $M_\odot$ for an OB star of this luminosity their mass loss prescription gives $\dot{M} = 10^{-5.69}\ M_\odot\ \mathrm{yr}^{-1}$ and $v_\infty = 2520$ km s^{-1} at solar metallicity. A reduction of v_∞ to 840 km s^{-1} leads to an increase of the mass loss rate by a factor of four, to $10^{-5.10}\ M_\odot\ \mathrm{yr}^{-1}$. A reduction of the stellar mass to 20 $M_\odot$ together with an adjustment of the Eddington factor to $\Gamma_e = 0.37$ further increases $\dot{M}$ by a factor of 1.5, to $\dot{M} = 10^{-4.91}\ M_\odot\ \mathrm{yr}^{-1}$. This is in exact agreement with the WNL model by Vink & de Koter (2005) with $\dot{M} = 10^{-4.89}\ M_\odot\ \mathrm{yr}^{-1}$. Because the Z-dependence also is the same, the models by Vink et al. (2001) thus closely resemble the WNL models by Vink & de Koter (2005).

According to Eqs. (3)–(6) our own models give a much lower value of $\dot{M} = 10^{-6.07}\ M_\odot\ \mathrm{yr}^{-1}$. Note, however, that our formula is not reliably applicable because the desired Eddington factor of 0.37 is very close to the parameter $\Gamma_0(Z_\odot) = 0.33$ (see the discussion at the end of Sect. 3.4). A direct model computation yields $\dot{M} = 10^{-5.4}\ M_\odot\ \mathrm{yr}^{-1}$ (see Table 2 for details). The discrepancy is caused by the influence of the He II continuum, which effectively increases the Eddington factor close to the critical point in this specific parameter range. Nevertheless, our mass loss rate is still significantly below the value from Vink & de Koter.

We conclude that our models are much more sensitive to the adopted Eddington factor than others. This leads to higher or lower mass loss rates, dependent on Γ_e. According to our models the proximity to the Eddington limit is the primary reason for the enhanced WR-type mass loss. This possibility has also been discussed by Vink & de Koter (2005). Our models however show qualitative changes in the optically thick regime that are also reflected in the Z-dependence of the mass loss. While the other studies find a universal relation with $\dot{M} \propto Z^{0.85}$ for almost all types of hot stars, we detect a flattening of the $\dot{M}(Z)$ relation for $\Gamma_e > 0.7$. For lower values of Γ_e our models show a similar Z-dependence to that determined by Vink & de Koter. The important fact that our models yield high mass loss rates over the whole range of metallicities implies that WR-type mass loss might gain importance in metal-poor environments (see the discussion in Sect. 5.6).

5. Discussion

In the preceding sections we have presented the first fully self-consistent models for the winds of WNL stars. These models reveal important information about the nature of these objects and their mass loss. In the following we discuss the most important points: the reason for their enhanced mass loss (Sect. 5.1), their evolutionary state (Sect. 5.2), the effect of wind clumping (Sect. 5.3), the role of radiative wind driving (Sect. 5.4), the Z-dependence of WR-type mass loss (Sect. 5.5), and its potential role in extremely metal-poor environments (Sect. 5.6).

5.1. What is the reason for WR-type mass loss?

The most important conclusion from our present work is that WR-type mass loss is primarily triggered by the proximity to the Eddington limit. As the main reason we identify the extension of the deep atmospheric layers, leading to the formation of

optically thick stellar winds. We have performed the first detailed computations of the atmospheric structure of such objects, and we have identified qualitative differences to OB star winds. The most important is the strong dependence of the mass loss rates on the Eddington factor Γ_e and on the effective stellar temperature $T_\star$. The idea that stellar mass loss increases close to the Eddington limit is of course not new. For example, for the case of LBVs Vink & de Koter (2002) also detected a strong dependence on Γ_e. Nevertheless, in stellar evolution models the surface composition and temperature are commonly used to discriminate between different states of mass loss.

The proximity to the Eddington limit provides a natural explanation for the occurrence of the WR phenomenon, for He-burning stars with their inherently high L/M ratios as well as for over-luminous H-burning stars. The latter is expected for very massive stars at the end of their main-sequence evolution and for fast rotators where fresh hydrogen is mixed into the stellar core (Meynet & Maeder 2000). Note that such objects are also expected to show WN surface compositions due to rotationally induced mixing and mass loss.

The wind driving in our present models mainly originates from line opacities of Fe III–VIII. These ions belong to the "cool" Fe opacity peak, in contrast to our previous WCE models, where the "hot" Fe peak (Fe IX–XVI) is responsible for the driving of the wind base (Gräfener & Hamann 2005). We thus confirm the prediction by Nugis & Lamers (2002) that the winds of WNL stars are driven by the cool Fe peak opacities, whereas for early spectral subtypes the critical point is located in much deeper layers where the hot Fe peak dominates.

5.2. The evolutionary status of WNL stars

The dichotomy among the WN subtypes, where the H-rich WNL stars show much higher luminosities than the earlier subtypes (e.g., Hamann et al. 2006), indicates that the progenitors of H-rich WNL stars are very massive stars with masses around 120 $M_\odot$. In Sect. 3.1 we have shown for the example of WR 22 (WN 7h) that the observed spectrum, including the absolute flux distribution, is reproduced by a very luminous model ($L_\star = 10^{6.3}\ L_\odot$) with $\Gamma_e = 0.55$, corresponding to a stellar mass of 78 $M_\odot$. Such a high mass implies that WR 22 is still in the phase of central H-burning. Our models thus suggest that, for very massive stars, the WNL phase might already occur at the end of the main-sequence evolution, when the L/M ratio increases due to the increase of the mean molecular weight in the stellar core.

Our parameters for WR 22 are in agreement with the evolutionary model for a rotating 120 $M_\odot$ star by Meynet & Maeder (2003), which is still in the phase of central H-burning (at an age of 2.2×10^6 yr). This means that our derived mass suggests that WR 22 is in the end phase of the main-sequence evolution. The observed mass loss rate of WR 22 ($10^{-4.85}\ M_\odot\,\mathrm{yr}^{-1}$) is not in agreement with the evolutionary models. In the models the mass loss switches from O-star mass loss (in the range of $10^{-5.0}$–$10^{-4.65}\ M_\odot\,\mathrm{yr}^{-1}$) to WNL mass loss ($\sim 10^{-4}\ M_\odot\,\mathrm{yr}^{-1}$) when the hydrogen surface mass fraction falls below 0.4. This sudden switch reduces the stellar mass very rapidly. The previous evolution of WR 22 has probably been different because, even with its present mass loss rate as the average value, it can only have lost up to 28 $M_\odot$ within 2 Myr.

Our models suggest an H-rich WNL phase at the end of the main sequence evolution of very massive stars. Within the standard evolutionary scenario such objects enter the LBV stage after leaving the main sequence (e.g., Crowther 2007). After losing their H-rich envelopes, they presumably evolve into the "classical" He-burning WR stages. Our models thus support an evolutionary sequence of the form O → WNL (H-rich) → LBV → WN (H-poor) → WC for very massive stars, as proposed by Langer et al. (1994). According to our results in Sect. 3.1, the mass loss from WNL stars increases strongly for decreasing stellar temperatures ($\dot{M} \propto T_\star^{-3.5}$). For temperatures below the values examined here, this might indeed lead to a smooth transition into the quiet LBV phase.

Additional evidence that the most massive stars are WNL stars comes from observations of young stellar clusters. There are several cases where the brightest stars in such clusters are WNL stars. A good example is the Carina OB cluster Tr 16 where only two evolved stars are present, the extremely luminous WNL star WR 25 (WN 6h, see Hamann et al. 2006) and η Car. Also the bright WNL stars in the Arches cluster (Najarro et al. 2004; Martins et al. 2008) and in R 136a (de Koter et al. 1997) fall into the same category as WR 22 and WR 25 – extremely luminous H-rich WNL stars with relatively weak emission lines. Moreover, the highest masses in binary systems are measured for WNL stars (Rauw et al. 1996; Schweickhardt et al. 1999; Bonanos et al. 2004; Moffat et al. 2007). H-rich WNL stars thus probably mark an important phase of strong mass loss at the end of the main-sequence evolution of very massive stars.

Note that we do not exclude the possibility of less luminous WNL stars being in the phase of central He-burning, succeeding a RSG/LBV phase. Our present assumption of high luminosities relies on galactic WNL stars with known distance, which are usually members of dense clusters. There are, however, many WNL stars that are not located in clusters, and that might have much lower luminosities. Such a case is WR 40 (WN 8h) which is located in the center of the ring nebula RCW 58, a possible remnant of a previous RSG outflow (see, e.g., Marston 1999).

5.3. The effect of wind clumping

Wind clumping is routinely taken into account in spectral analyses of WR stars. Its main effect is that the mean $\langle\rho^2\rangle$ increases and thus the derived mass loss rates, relying on ρ^2-diagnostics, decrease with $\dot{M} \propto 1/\sqrt{D}$ (see Hamann & Koesterke 1998a). In the present work we have shown that clumping also affects the wind acceleration. The reason for this is that excited energy levels are more populated by recombination processes. For the dense winds of WR stars, the resulting increase of optically thin lines leads to an increase of the radiative acceleration, approximately with $a_{\rm rad} \propto \sqrt{D}$. Moreover, the force multiplier parameter α is reduced. At this point it is necessary to emphasize that we assume small-scale clumps (micro-clumping) in our models. In this limit the separation between clumps is so small that the mean opacity can be used in the radiative transfer. In the limit of large clump separation (macro-clumping) the optical depth of individual clumps may become large. Brown et al. (2004) have shown that in this case the radiative acceleration is reduced by geometrical effects. With a modified approach for the wind opacity Oskinova et al. (2007) have shown that spectral diagnostics also are considerably affected by macro-clumping.

We thus have two counteracting effects that may affect our results. Micro-clumping increases the radiative acceleration with $a_{\rm rad} \propto \sqrt{D}$, and macro-clumping decreases $a_{\rm rad}$ dependent on the detailed clump-geometry. In our present models only micro-clumping is taken into account. We have shown that it only affects the wind speed as long as it is restricted to the outer wind region above the critical point. In some of our models the

critical region is however marginally affected by clumping. This of course introduces an uncertainty in our mass loss rates.

Note that significant clumping factors in the range of $D = 10-100$ have recently been proposed for OB star winds (Crowther et al. 2002; Hillier et al. 2003; Bouret et al. 2003, 2005; Fullerton et al. 2006). If the effects of micro-clumping dominate, the observed mass loss rates of OB stars thus should be revised downward by factors of 3−10. This would of course introduce a discrepancy in the previous wind models for OB stars because these do not take clumping into account. As we discussed in Sect. 4.3, our models yield a much lower radiative force than others, which seems to be connected to the detailed CMF radiative transfer. In contrast to the standard Sobolev models, spectral lines have a finite width in our approach. Interestingly, Lucy (2007) has proposed that the assumption of infinitely narrow spectral lines leads to an over-estimation of the mass loss rates in the standard models, i.e., OB star mass loss rates should actually be lower. Because of its influence on the wind dynamics and the wind diagnostics, it thus seems that clumping is fundamentally important for the physics of radiatively driven winds. Because the actual mechanisms of wind clumping are presently not well understood, it introduces significant uncertainties in all types of mass loss predictions for hot stars.

5.4. Are WR winds generally driven by radiation?

In the present work we have shown that WNL star winds can be explained self-consistently by pure radiative driving. As the reason for their strong optically thick winds we have identified the extension of the deep atmospheric layers due to the radiative force on Fe line opacities. For our present WNL models the cool Fe-peak opacities are responsible for this effect. Together with our previous results for early-type WC stars (Gräfener & Hamann 2005), where the inner wind is driven by the hot Fe-peak, one might now argue that WR winds are generally driven by radiation. This would imply a general Z-dependence of WR mass loss.

The fact that the two Fe opacity peaks act in different temperature regimes, however, has important consequences for our models. First, because of the gap between the two peaks, the mass loss cannot be maintained for intermediate stellar temperatures ($T_\star = 60-100$ kK). Second, for cool objects, the hot Fe-peak disturbs the inner atmospheric structure.

The first point is connected to the well-known "extension problem" of H-free WR stars. For H-free WN and WC stars stellar structure models predict much smaller radii than observed. Note that the predicted radii correspond to stellar temperatures above ~100 kK, in agreement with our wind models. Observed stellar temperatures, however, extend down to ~50 kK (e.g. Hamann et al. 2006). From a theoretical point of view such objects are thus not expected to exist, and they are not expected to have WR-type stellar winds. Ishii et al. (1999) have shown that very luminous WR stars might form an extended convection zone close to the stellar surface which can account for the observed extension. According to Petrovic et al. (2006) this extension however only occurs under the assumption of hydrostatic equilibrium. As soon as dynamic terms are included in their computations the extension disappears. Interestingly, this extension is caused by the hot Fe-peak. According to our computations the hot Fe-peak drives the stellar wind, i.e., the possible extension of the outer layers of WR stars is hindered by their mass loss. A possible solution for this problem could be the pulsational driving of the deep layers (e.g., by strange mode instabilities as proposed by Glatzel & Kaltschmidt 2002). This could help to overcome the opacity-gap between the two Fe-peaks, and also account for the observed extension. Another possibility would be to bring the stars closer to the Eddington limit. For He-burning stars the L/M ratio is however fixed. As also discussed by Vink & de Koter (2005), fast stellar rotation may help to reduce the surface gravity of such objects and initiate strong mass loss. That this process works for optically thick winds, however, remains to be shown. For OB star winds Madura et al. (2007) have demonstrated that rotation increases the mass loss at most by a factor of two.

The second problem only arises for late spectral subtypes. For these stars the cool Fe-peak drives the stellar wind, and the hot Fe-peak is located in deep layers at temperatures around 160 kK. For a star close to the Eddington limit it can thus happen that the radiative force exceeds gravity in the deep hydrostatic layers. In the stellar interior this would lead to the onset of convection. Particularly for stars with dense winds this situation already occurs at the inner boundary of our atmosphere models. We thus reach a mass loss limit above which we cannot obtain stationary wind models. In reality this presumably leads to a non-stationary situation. Dorfi et al. (2006) have recently shown that the observed variability in WN 8 subtypes can indeed be explained by instabilities that are caused by the hot Fe-peak.

The comparison with observations in Sect. 3.1 has shown that only a part of the galactic WR sample is reproduced by our models. The WN 8 subtypes particularly have higher wind densities than predicted. The comparison with the WN 8 model from Vink & de Koter (2005) in Sect. 4.3 has shown that this problem still holds if lower luminosities are adopted. According to our models a different driving mechanism thus would be desirable, at least for the wind base of these objects. Again, this mechanism could be related to the observed pulsations (see e.g. Marchenko et al. 1998; Lefèvre et al. 2005) or rotational driving. Note that also the non-detection of X-ray emission from WN 8 subtypes might be a hint to a different wind driving mechanism (see Oskinova 2005).

5.5. The Z-dependence of WR mass loss

As expected for radiatively driven winds, our models show a strong Z-dependence. Because of the important influence of the Eddington factor, it is however not sufficient to parametrize the mass loss as a function of Z alone. In Sect. 3.4 we have thus prepared a mass loss recipe which takes the combined effect of Γ_e and Z into account. According to Eqs. (4)−(6) the metallicity Z affects the resulting mass loss rates in two ways. First, the parameter $\Gamma_0(Z)$ decreases for increasing Z (Eq. (6)). Γ_0 characterizes the limiting Eddington factor for which WR-type mass loss sets in. An increasing metallicity thus brings the star effectively closer to the Eddington limit, and supports the formation of WR-type winds. Second, the exponent $\beta(Z)$ increases with Z (Eq. (5)). This results in the flattening of the $\dot{M}(Z)$ relation for low Z and large Γ_e (see Sect. 4.3).

A higher metallicity thus has two effects. The mass loss from WR stars increases and WR stars are formed more easily. According to our models, at solar metallicity the most massive stars already enter the WNL phase at the end of the H-burning stage. For $Z = 3\ Z_\odot$ we could even show that stars with 120 $M_\odot$ already become WNL stars on the zero-age main sequence (Gräfener & Hamann 2006). In low metallicity environments, on the other hand, the occurrence of WR-type winds should be restricted to He-burning objects and maybe to fast rotators. The influence of metallicity on WR populations is thus

extremely complex. In different environments different objects become WR stars.

5.6. WR-type mass loss in extremely metal-poor environments

In Sect. 4.3 we have shown that the slope of the $\dot{M}(Z)$ relation becomes shallower for increasing Γ_e. Close to the Eddington limit our models are thus able to produce large mass loss rates also at very low Z. Note that these are presently the only wind models for low metallicities for which such an efficient mass loss mechanism has been detected. The large Eddington factors that are required ($\Gamma_e \approx 0.8$) are however only reached by very massive objects or stars close to critical rotation. Both types of objects are indeed expected at low Z (see also the discussion in Vink & de Koter 2005). For extremely low metallicities ($Z < 10^{-4}\ Z_\odot$) more massive stars are expected to form (Bromm et al. 1999; Nakamura & Umemura 2002). Moreover, evolutionary calculations indicate that rotating massive stars tend to approach critical rotation more easily at low Z (Meynet & Maeder 2002). Our present models show that high mass loss rates can be maintained in this regime, and that such objects should appear as WR stars with particularly low wind velocities. Note, however, that the question of whether rotation really leads to increased mass loss remains to be investigated in more detail. For CAK-type winds Madura et al. (2007) recently demonstrated that rotation increases $\dot{M}$ at most by a factor of two.

A new and very important result from our calculations concerns the role of primary elements for the wind driving of extremely metal-poor stars. Yoon & Langer (2005), as well as Meynet et al. (2006), have shown that rotating massive stars at extremely low Z ($10^{-5}\ Z_\odot$ and $10^{-8}\ Z_\odot$ respectively) are capable of producing nitrogen mass fractions in the range of one percent at their surface. The mass loss from such objects may potentially enrich the early ISM with freshly produced nitrogen. With the adopted stellar yields from Meynet et al. (2006), Chiappini et al. (2006) could explain the observed high nitrogen abundances in extremely metal-poor halo stars (Spite et al. 2005).

Our iron-free models in Sect. 3.3 now confirm that such self-enriched objects can develop strong stellar winds. We find that iron-free objects with solar Z (i.e., $X_{\rm CNO} = Z_\odot$ and $X_{\rm Fe} = 0$) can reach mass loss rates similar to stars with standard composition at $Z_\odot/50$. This means that medium-complex elements like C, N, and O are much less efficient for the wind driving than the complex Fe-group elements. For more realistic mass loss predictions it is thus important to take the relative contributions of different elements into account.

For the application of Z-dependent mass loss relations like our Eqs. (4)–(6), we thus suggest the use of an effective metallicity $Z_{\rm eff}$, where the relative contributions of different elements are adequately weighted. In the present case of CNO-enriched WNL stars we propose an approximation of the form

$$Z_{\rm eff} \approx Z_\odot \cdot \left(\frac{1}{50} \frac{X_{\rm CNO}}{X_{\rm CNO,\odot}} + \frac{X_{\rm Fe}}{X_{\rm Fe,\odot}} \right). \quad (7)$$

6. Conclusions

We have performed a systematic study of the mass loss from late-type WN stars by means of a new generation of non-LTE atmosphere models, including a self-consistent treatment of the wind hydrodynamics. This was the first application of these complex models on a large scale. We could show that the strong winds from WNL stars can be explained self-consistently by radiative driving, and that the proximity to the Eddington limit is the primary trigger of the enhanced WR-type mass loss. Moreover we have identified important qualitative differences to OB star winds that are caused by the altered wind physics.

Our models reproduce the observed sequence of late spectral subtypes from WN 6 to WN 9 qualitatively. The obtained wind densities are in agreement with the galactic WNL sample, except for the enigmatic WN 8 subtypes with strong winds. A detailed comparison with the spectroscopic binary WR 22 supports our key statement that H-rich WNL stars are very massive, luminous stars close to the Eddington limit. Our models imply that these objects are still in the phase of central H-burning, in line with an evolutionary sequence of the form O → WNL (H-rich) → LBV → WN (H-poor) → WC for very massive stars (e.g., Langer et al. 1994; Crowther 2007). Due to the strong temperature-dependence of the mass loss ($\dot{M} \propto T_\star^{-3.5}$), an evolution towards cooler effective temperatures may indeed lead to a continuous transition into the quiet LBV phase.

As expected for radiatively driven winds, our models show a strong Z-dependence. The influence of the Eddington factor Γ_e however is at least equally important. We find that the $\dot{M}(Z)$ relation for WNL stars becomes flatter for higher Γ_e, i.e., high mass loss rates can also be maintained for very low Z. Our models thus predict an efficient mass loss mechanism for low metallicity stars. For stars in extremely metal-poor environments (i.e. the second generation of massive stars) we find that the surface-enrichment with primary nitrogen, as described, e.g. by Meynet et al. (2006), may lead to strong mass loss. We thus confirm that these first WN stars might play a key role in the enrichment of the early ISM with freshly produced nitrogen.

References

Abbott, D. C. 1982, ApJ, 259, 282
Anderson, L. S. 1989, ApJ, 339, 558
Auer, L. H., & Mihalas, D. 1970, MNRAS, 149, 65
Barniske, A., Hamann, W.-R., & Gräfener, G. 2006, in Stellar Evolution at Low Metallicity: Mass Loss, Explosions, Cosmology, ed. H. J. G. L. M. Lamers, N. Langer, T. Nugis, & K. Annuk, ASP Conf. Ser., 353, 243
Bonanos, A. Z., Stanek, K. Z., Udalski, A., et al. 2004, ApJ, 611, L33
Bouret, J.-C., Lanz, T., & Hillier, D. J. 2005, A&A, 438, 301
Bouret, J.-C., Lanz, T., Hillier, D. J., et al. 2003, ApJ, 595, 1182
Bromm, V., Coppi, P. S., & Larson, R. B. 1999, ApJ, 527, L5
Brown, J. C., Cassinelli, J. P., Li, Q., Kholtygin, A. F., & Ignace, R. 2004, A&A, 426, 323
Castor, J. I., Abbott, D. C., & Klein, R. I. 1975, ApJ, 195, 157
Chiappini, C., Hirschi, R., Meynet, G., et al. 2006, A&A, 449, L27
Conti, P. S., Garmany, C. D., & Massey, P. 1989, ApJ, 341, 113
Crowther, P. A. 2000, A&A, 356, 191
Crowther, P. A. 2007, ARA&A, 45, 177
Crowther, P. A., & Dessart, L. 1998, MNRAS, 296, 622
Crowther, P. A., Hillier, D. J., Evans, C. J., et al. 2002, ApJ, 579, 774
Cunto, W., & Mendoza, C. 1992, Rev. Mex. Astron. Astrofis., 23, 107
Davidson, K., Smith, N., Gull, T. R., Ishibashi, K., & Hillier, D. J. 2001, AJ, 121, 1569
de Koter, A., Heap, S. R., & Hubeny, I. 1997, ApJ, 477, 792
Dorfi, E. A., Gautschy, A., & Saio, H. 2006, A&A, 453, L35
Fitzpatrick, E. L. 1999, PASP, 111, 63
Fullerton, A. W., Massa, D. L., & Prinja, R. K. 2006, ApJ, 637, 1025
Glatzel, W., & Kaltschmidt, H. O. 2002, MNRAS, 337, 743
Gosset, E., Remy, M., Manfroid, J., et al. 1991, Informational Bulletin on Variable Stars, 3571, 1
Gräfener, G., & Hamann, W.-R. 2003, in A Massive Star Odyssey: From Main Sequence to Supernova, ed. K. A. van der Hucht, A. Herrero, & E. César (San Francisco: ASP), IAU Symp., 212, 190
Gräfener, G., & Hamann, W.-R. 2005, A&A, 432, 633
Gräfener, G., & Hamann, W.-R. 2006, in The Metal Rich Universe, ed. G. Israelian, to appear [arXiv:astro-ph/0609672]

Gräfener, G., Hamann, W.-R., & Koesterke, L. 2000, in Thermal and Ionization Aspects of Flows from Hot Stars, ed. H. J. G. L. M. Lamers, & A. Sapar (San Francisco: ASP), ASP Conf. Ser., 204, 215
Gräfener, G., Koesterke, L., & Hamann, W.-R. 2002, A&A, 387, 244
Hamann, W.-R. 1981, A&A, 93, 353
Hamann, W.-R. 1985, A&A, 148, 364
Hamann, W.-R. 1986, A&A, 160, 347
Hamann, W.-R., & Koesterke, L. 1998a, A&A, 335, 1003
Hamann, W.-R., & Koesterke, L. 1998b, A&A, 333, 251
Hamann, W.-R., & Gräfener, G. 2003, A&A, 410, 993
Hamann, W.-R., & Gräfener, G. 2004, A&A, 427, 697
Hamann, W.-R., Leuenhagen, U., Koesterke, L., & Wessolowski, U. 1992, A&A, 255, 200
Hamann, W.-R., Peña, M., Gräfener, G., & Ruiz, M. T. 2003, A&A, 409, 969
Hamann, W.-R., Gräfener, G., & Liermann, A. 2006, A&A, 457, 1015
Herald, J. E., Hillier, D. J., & Schulte-Ladbeck, R. E. 2001, ApJ, 548, 932
Hillier, D. J. 2003, in A Massive Star Odyssey, From Main Sequence to Supernova, ed. K. A. van der Hucht, A. Herrero, & E. César (San Francisco: ASP), IAU Symp., 212, 70
Hillier, D. J., & Miller, D. L. 1998, ApJ, 496, 407
Hillier, D. J., Lanz, T., Heap, S. R., et al. 2003, ApJ, 588, 1039
Howarth, I. D., & Schmutz, W. 1992, A&A, 261, 503
Hummer, D. G., & Mihalas, D. 1988, ApJ, 331, 794
Iglesias, C. A., & Rogers, F. J. 1996, ApJ, 464, 943
Ishii, M., Ueno, M., & Kato, M. 1999, PASJ, 51, 417
Koesterke, L., & Hamann, W.-R. 1995, A&A, 299, 503
Koesterke, L., Hamann, W.-R., & Kosmol, P. 1992, A&A, 255, 490
Koesterke, L., Hamann, W.-R., & Gräfener, G. 2002, A&A, 384, 562
Krtička, J., & Kubát, J. 2004, A&A, 417, 1003
Kudritzki, R. P., Puls, J., Lennon, D. J., et al. 1999, A&A, 350, 970
Kurucz, R. L. 1991, in Stellar Atmospheres – Beyond Classical Models, ed. L. Crivellary, I. Hubeny, & D. G. Hummer, NATO ASI Ser., 341, 441
Kurucz, R. L. 2002, in Atomic and Molecular Data and Their Applications, AIP Conf. Proc., 636, 134
Kurucz, R. L., & Bell, B. 1995, Kurucz CD-ROM No. 23 (Cambridge, Mass.: Smithsonian Astrophysical Observatory)
Lamers, H. J. G. L. M., & Nugis, T. 2002, A&A, 395, L1
Lamers, H. J. G. L. M., Snow, T. P., & Lindholm, D. M. 1995, ApJ, 455, 269
Langer, N., Hamann, W.-R., Lennon, M., et al. 1994, A&A, 290, 819
Lefèvre, L., Marchenko, S. V., Moffat, A. F. J., et al. 2005, ApJ, 634, L109
Leuenhagen, U., & Hamann, W.-R. 1994, A&A, 283, 567
Leuenhagen, U., Hamann, W.-R., & Jeffery, C. S. 1996, A&A, 312, 167
Lucy, L. B. 1964, in First Harvard-Smithsonian Conference on Stellar Atmospheres, ed. E. H. Avrett, O. J. Gingerich, & C. A. Whitney, Smithsonian Astrophysical Observatory Special Report No. 167 (Cambridge, Mass.), 93
Lucy, L. B. 2007, A&A, 468, 649
Lucy, L. B., & Abbott, D. C. 1993, ApJ, 405, 738
Lundström, I., & Stenholm, B. 1984, A&AS, 58, 163
MacFadyen, A. I., & Woosley, S. E. 1999, ApJ, 524, 262
Madura, T. I., Owocki, S. P., & Feldmeier, A. 2007, ApJ, 660, 687
Marchenko, S. V., Moffat, A. F. J., Eversberg, T., et al. 1998, MNRAS, 294, 642
Marston, A. P. 1999, in Wolf-Rayet Phenomena in Massive Stars and Starburst Galaxies, ed. K. A. van der Hucht, G. Koenigsberger, & P. R. J. Eenens, IAU Symp., 193, 306
Martins, F., Hillier, D. J., Paumard, T., et al. 2008, A&A, 478, 219
Massey, P., & Johnson, J. 1993, AJ, 105, 980
Meynet, G., & Maeder, A. 2000, A&A, 361, 101
Meynet, G., & Maeder, A. 2002, A&A, 390, 561
Meynet, G., & Maeder, A. 2003, A&A, 404, 975
Meynet, G., Ekström, S., & Maeder, A. 2006, A&A, 447, 623
Mihalas, D., Kunasz, P. B., & Hummer, D. G. 1976, ApJ, 206, 515
Moffat, A. F. J., Schnurr, O., Chené, A.-N., et al. 2007, Highlights of Astronomy, 14, 197
Mokiem, M. R., de Koter, A., Puls, J., et al. 2005, A&A, 441, 711
Mokiem, M. R., de Koter, A., Evans, C. J., et al. 2007a, A&A, 465, 1003
Mokiem, M. R., de Koter, A., Vink, J. S., et al. 2007b, A&A, 473, 603
Nahar, S. N. 1999, ApJS, 120, 131
Nahar, S. N., & Pradhan, A. K. 1997, ApJS, 111, 339
Najarro, F., Figer, D. F., Hillier, D. J., & Kudritzki, R. P. 2004, ApJ, 611, L105
Nakamura, F., & Umemura, M. 2002, ApJ, 569, 549
Niedzielski, A., & Skorzynski, W. 2002, Acta Astron., 52, 81
Nugis, T., & Lamers, H. J. G. L. M. 2002, A&A, 389, 162
Oskinova, L. M. 2005, MNRAS, 361, 679
Oskinova, L. M., Hamann, W. R., & Feldmeier, A. 2007, ArXiv e-prints, 704
Pauldrach, A. W. A., Hoffmann, T. L., & Lennon, M. 2001, A&A, 375, 161
Petrovic, J., Pols, O., & Langer, N. 2006, A&A, 450, 219
Pistinner, S., & Eichler, D. 1995, ApJ, 454, 404
Puls, J., Springmann, U., & Lennon, M. 2000, A&AS, 141, 23
Rauw, G., Vreux, J.-M., Gosset, E., et al. 1996, A&A, 306, 771
Schmutz, W. 1997, A&A, 321, 268
Schweickhardt, J., Schmutz, W., Stahl, O., Szeifert, T., & Wolf, B. 1999, A&A, 347, 127
Seaton, M. 1987, J. Phys. B (Atom. Mol. Phys.), 20, 6363
Seaton, M. J., Yan, Y., Mihalas, D., & Pradhan, A. K. 1994, MNRAS, 266, 805
Seaton, M. J., Zeippen, C. J., Tully, J. A., et al. 1992, Rev. Mex. Astron. Astrofis., 23, 19
Spite, M., Cayrel, R., Plez, B., et al. 2005, A&A, 430, 655
Springmann, U. 1994, A&A, 289, 505
Stasińska, G., Gräfener, G., Peña, M., et al. 2004, A&A, 413, 329
The Opacity Project Team 1995, The Opacity Project (Bristol, UK: Institute of Physics Publications), 1
Unsöld, A. 1955, Physik der Sternatmosphären, 2nd edn. (Berlin: Springer Verlag)
van der Hucht, K. A. 2001, New Astron. Rev., 45, 135
Vink, J. S., & de Koter, A. 2002, A&A, 393, 543
Vink, J. S., & de Koter, A. 2005, A&A, 442, 587
Vink, J. S., de Koter, A., & Lamers, H. J. G. L. M. 2000, A&A, 362, 295
Vink, J. S., de Koter, A., & Lamers, H. J. G. L. M. 2001, A&A, 369, 574
Woosley, S., & Heger, A. 2006, ApJ, 637, 914
Woosley, S. E., Langer, N., & Weaver, T. A. 1993, ApJ, 411, 823
Yoon, S.-C., & Langer, N. 2005, A&A, 443, 643